

1-1-1988

## Measurement of the nitrogen(+) ((5)sulfide) state radiative lifetime

Jianzhong Jiang  
*University of Nevada, Las Vegas*

Follow this and additional works at: <https://digitalscholarship.unlv.edu/rtds>

---

### Repository Citation

Jiang, Jianzhong, "Measurement of the nitrogen(+) ((5)sulfide) state radiative lifetime" (1988). *UNLV Retrospective Theses & Dissertations*. 55.  
<http://dx.doi.org/10.25669/wixg-mika>

This Thesis is protected by copyright and/or related rights. It has been brought to you by Digital Scholarship@UNLV with permission from the rights-holder(s). You are free to use this Thesis in any way that is permitted by the copyright and related rights legislation that applies to your use. For other uses you need to obtain permission from the rights-holder(s) directly, unless additional rights are indicated by a Creative Commons license in the record and/or on the work itself.

This Thesis has been accepted for inclusion in UNLV Retrospective Theses & Dissertations by an authorized administrator of Digital Scholarship@UNLV. For more information, please contact [digitalscholarship@unlv.edu](mailto:digitalscholarship@unlv.edu).

## INFORMATION TO USERS

The most advanced technology has been used to photograph and reproduce this manuscript from the microfilm master. UMI films the text directly from the original or copy submitted. Thus, some thesis and dissertation copies are in typewriter face, while others may be from any type of computer printer.

The quality of this reproduction is dependent upon the quality of the copy submitted. Broken or indistinct print, colored or poor quality illustrations and photographs, print bleedthrough, substandard margins, and improper alignment can adversely affect reproduction.

In the unlikely event that the author did not send UMI a complete manuscript and there are missing pages, these will be noted. Also, if unauthorized copyright material had to be removed, a note will indicate the deletion.

Oversize materials (e.g., maps, drawings, charts) are reproduced by sectioning the original, beginning at the upper left-hand corner and continuing from left to right in equal sections with small overlaps. Each original is also photographed in one exposure and is included in reduced form at the back of the book. These are also available as one exposure on a standard 35mm slide or as a 17" x 23" black and white photographic print for an additional charge.

Photographs included in the original manuscript have been reproduced xerographically in this copy. Higher quality 6" x 9" black and white photographic prints are available for any photographs or illustrations appearing in this copy for an additional charge. Contact UMI directly to order.



University Microfilms International  
A Bell & Howell Information Company  
300 North Zeeb Road, Ann Arbor, MI 48106-1346 USA  
313/761-4700 800/521-0600



Order Number 1338263

**Measurement of the  $N^+ \ ^5S_2$  state radiative lifetime**

**Jiang, Jianzhong, M.S.**

University of Nevada, Las Vegas, 1989

**U·M·I**  
300 N. Zeeb Rd.  
Ann Arbor, MI 48106



MEASUREMENT OF THE  $N^+ 5S_2$  STATE RADIATIVE LIFETIME

By

Jianzhong Jiang

A thesis submitted in partial fulfillment  
of the requirements for the degree of

Master of Science

in

Physics

Department of Physics

University of Nevada, Las Vegas

March, 1989

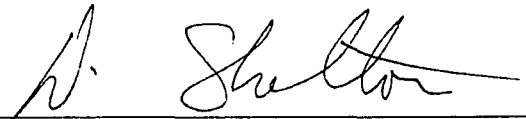
The thesis of Jianzhong Jiang for the degree of Maser of Science in Physics is approved.



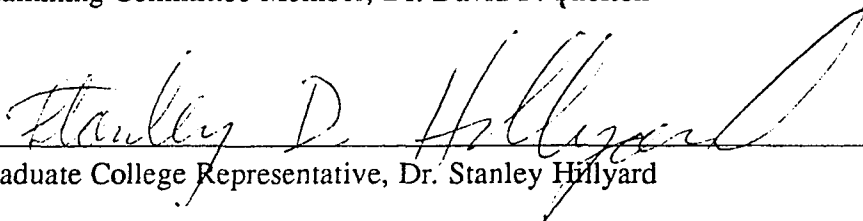
Chairperson, Dr. Victor H.S. Kwong



Examining Committee Member, Dr. James C. Selser



Examining Committee Member, Dr. David P. Shelton



Graduate College Representative, Dr. Stanley Hillyard



Graduate Dean, Dr. Ronald W. Smith

University of Nevada Las Vegas  
Las Vegas, Nevada  
June 1989

# MEASUREMENT OF THE $N^+ 5S_2$ STATE RADIATIVE LIFETIME

by

Jianzhong Jiang

## ABSTRACT

The radiative lifetime of metastable  $N^+(2s2p^3 5S_2)$  has been measured by directly monitoring the spontaneous emission from stored  $N^+$  in a radio-frequency ion trap. The electron excitation technique was used to create  $N^+(5S_2)$ , and the spontaneous emission decay curve via spin-forbidden electric dipole transitions from  $2s2p^3 5S_2$  to  $2s^22p^2 3P_{1,2}$  ground state at 2139.68 and 2143.55 Å were observed. A measured value for the  $5S_2$  radiative lifetime is

$$\tau_{\text{rad}} = 6.4 \pm 0.7 \text{ ms}$$

which is in good agreement with the theoretical result by Hibbert and Bates but longer than the measurement by Knight ( $4.2 \pm 0.6 \text{ ms}$ ). A careful study of non-radiative quenching and ion loss due to charge transfer of the metastable state was made. It was found that Knight's results were non-reproducible at a higher vacuum system with a meshed wall ion trap. This is perhaps due to unknown impurity gases in Knight's vacuum system. This measurement will clarify the discrepancy between Knight's measurement and theoretical calculations. An accurate value for the lifetime of the metastable  $N^+(2s2p^3 5S_2)$  ion is important in interpretation of the UV spectra of aurora.



## TABLE OF CONTENTS

Title	
Approval	
Abstract	i
Table of Contents	ii
Figure Captions	iii
Acknowledgements	vi
I. Introduction	1
II. Theoretical Outline	4
A. The Physics of Many–Electron atoms(ions)	4
B. Calculation of the $N^+(^5S_2)$ Radiative Lifetime	8
III. Experimental Facilities	9
1) The Vacuum System and Vacuum Chamber Configuration	9
2) The RF–Quadrupole Ion Trap	13
3) Electron Gun and Channel Electron Multiplier	21
A. Electron Gun	21
B. Channel Electron Multiplier	23
4) The Photon Detection System	23
5) Control Process Unit – The Experimental Timing Control Box	25
6) Data Analysis System	27
IV. Experimental Method and Procedures	29
1) Experimental Method and General Procedures	29
2) Creation of $N^+$	31
3) Ion Selection and Storage	35

	iii
4) Photon Detection	41
5) Data Analysis	41
V. Experimental Results	43
VI. Conclusion	49
References	50

## FIGURE CAPTIONS

	Page
Fig.(1) Block diagram of the $N^+(^5S_2)$ lifetime experiment	10
Fig.(2) The vacuum system	11
Fig.(3) The vacuum chamber configuration	12
Fig.(4) Configuration of the ion trap	14
Fig.(5) Geometry of the RF-Quadrupole ion trap	16
Fig.(6) Stability diagram of the ion trap	18
Fig.(7) Contours of the number of ions stored	22
Fig.(8) Photon detection system	24
Fig.(9) Photomultiplier Tube spectral response	26
Fig.(10) Experimental timing and control signals	30
Fig.(11) The CPU e gun signal, relax signal combined with the dual regulated power supply's response signal	33
Fig.(12) The residual gas composition	34
Fig.(13) a. Calculated results show that at $V_o = 400V$ , $f_o = 1.2MHz$ , $U_o = 25V$ $N^+$ ions are in the largest density area whereas $N_2^+$ and $N^{+2}$ can not be confined b. $N^+$ signal detected by channel electron multiplier at $V_o = 400V$ , $f_o = 1.2MHz$ , $U_o = 25V$	36
Fig.(14) a. Calculated results show that at $V_o = 255V$ , $f_o = 0.65MHz$ , $U_o = 20V$ , only $N_2^+$ can be trapped b. $N_2^+$ signal detected by channel electron multiplier at $V_o = 255V$ , $f_o = 0.65MHz$ , $U_o = 20V$	37
Fig.(15) a. Calculated results show that at $V_o = 220V$ ,	

$f_o = 0.65\text{MHz}$ ,  $U_o = 20\text{V}$ , both  $\text{N}^+$  and  $\text{N}_2^+$  can be confined

- b.  $\text{N}^+$  and  $\text{N}_2^+$  signal detected by channel electron multiplier at  $V_o = 220\text{V}$ ,  $f_o = 0.65\text{MHz}$ ,  
 $U_o = 20\text{V}$

38

Fig.(16) The decay curves of  $\text{N}^+$  signal vs storage time under various  $\text{N}_2$  pressure. The signals have been normalized

40

Fig.(17) A typical  $\text{N}^+(\text{}^5\text{S}_2)$  decay curve. The straight line is the least-squares analysis of this decay

44

Fig.(18)  $\text{N}^+$  decay rate vs  $\text{N}_2$  pressure. The slope of the decay rate vs  $\text{N}_2$  pressure gives a nonradiative quenching plus ion loss rate coefficient of  $1.14 \times 10^{-9}\text{cm}^3\text{sec}^{-1}$  and zero extrapolation gives  $\text{N}_2^+(\text{}^5\text{S}_2)$  decay rate  $A_{\text{rad}} = 156 \pm 17 \text{ sec}^{-1}$ .

46

## ACKNOWLEDGEMENTS

I wish to thank many people who have helped me with this work. I am grateful to Dr. Victor H. S. Kwong, my thesis adviser, for his guidance and constant support. I also thank my thesis examining committee members Dr. James C. Selser, Dr. David P. Shelton and the Graduate College Representative Dr. Stanley Hillyard for their detailed review and helpful suggestions. Discussions with Dr. John W. Farley and Dr. Zuyun Fang have been very helpful.

I want to express special appreciation to Terrence Gibbons and Heinz Knocke for their technical assistance with this experiment from beginning to end.

Many thanks to Dr. Stanley D. Cloud, Judy Earl, Bruce Rugar, Steve Huang and Emilio Braganza for their encouragement, help and friendship. The enthusiastic assistance of Monty Mckiernan and Johannes K. Schaller is also appreciated.

I also wish to thank the Graduate College for the Silver Dragon Scholarship.

Finally, but most important, I wish to express my deepest gratitude to my wife, Luxia; my son, Sirui; as well as my parents and hostfamily for the understanding, patience and aid given to me throughout this work and preceding university education.

This work was supported in part by the National Science Foundation (EPSCOR) RII-8410674 to the University of Nevada System, the Joseph H. deFrees Grant of the Research Corporation and the UNLV Research Council.

## I INTRODUCTION

The determination of atomic transition probabilities and lifetimes is an active research area. Various new experimental and theoretical methods have been developed in recent years. New research areas have opened up and the accuracy of the numerical data has significantly improved to meet the increasing demand to understand the basic structure of matter and to create new techniques and devices.<sup>1</sup>

Major applications for atomic transition probabilities and atomic lifetimes exist in the following fields:

(1) Astrophysics:

To determine the stellar element abundances, where transition probabilities are the key atomic parameters

(2) Space physics:

Space astronomers need the transition probability data to interpret the far-ultraviolet and soft x-ray spectral line emission from highly ionized species in the solar corona.

(3) Upper atmosphere physics (aeronomy)

Accurate transition probability data for the atmospheric gases are needed for the study of upper atmosphere processes.

(4) Plasma physics, gaseous discharges:

Transition probabilities of stable gases are of interest in the diagnostics of plasmas as well as studies of equilibrium states.

(5) Thermonuclear fusion research

In very hot plasmas, minute heavy element impurities from highly stripped ions radiate large amounts of energy away and thus contribute appreciably to plasma cooling. This is a critical problem in thermonuclear fusion. To analyze and model these energy-loss

problems, data for highly stripped ions of wall materials like Cr, Fe, Ni, Mo, and W are needed.

#### (6) Development of laser systems

Atomic transition probabilities and radiative decay rates of atomic levels are very important parameters needed to assess the potential of a system as a laser, since population inversions can be achieved only if some basic relationships and inequalities are satisfied among these quantities.

This thesis focuses on an experiment that measures  $N^+(2s2p^3\ ^5S_2)$  ion decay via spin-orbit induced electric dipole transitions to the  $2s^22p^2\ ^3P_{1,2}$  ground state at wavelengths of  $2139.68\text{\AA}$  and  $2143.55\text{\AA}$  respectively. This spontaneous decay is believed to be the origin of the  $\lambda\ 2145\text{\AA}$  auroral feature.<sup>2, 3, 4, 5</sup> It is known that auroras are produced by fast ions from the sun that interact with the earth's atmospheric oxygen and nitrogen. Atmospheric molecules such as  $N_2$  are ionized and excited by these fast ions. Those excited ions then decay, radiating light in the characteristic wavelengths of the particular elements.

Considerable interest attaches to the study of the excitation and ionization effects produced in nitrogen by electron impact.<sup>2, 3, 4, 5, 6, 7, 8</sup> This is partly due to the interpretation of the strong auroral feature near  $\lambda\ 2145\text{\AA}$ .

Theoretical studies of the  $N^+(\ ^5S_2)$  radiative lifetime were done years ago. A purely theoretical calculation, done by Hibbert and Bates,<sup>5</sup> yields a lifetime of 6.4 ms. Dalgarno, Victor and Hartquist<sup>4</sup> extrapolated along the carbon isoelectronic sequence, using previously calculated transition rates for higher ionization states, and obtained a lifetime of 5.8 ms. On the other hand, laboratory study by Knight,<sup>3</sup> who measured radiative lifetime of  $N^+(\ ^5S_2)$  ions, gave a lifetime of  $4.2 \pm 0.6$  ms. This value is about 34% off from the theoretical calculations. Measurement by Kwong and Johnson (1982),<sup>9</sup> and Calamai (1988)<sup>10</sup> consistently gave a higher value

of  $5.67 \pm 0.17$  ms and  $5.7 \pm 0.6$  ms respectively. It is hoped that this experiment will resolve the discrepancy among these measurements.

This thesis is divided into several parts. Before presenting experimental details, it will give a theoretical background of many-electron atoms (ions) and a brief description of approximate calculation for the lifetime. Following that the experimental facilities will be introduced and the experiment methods and procedures will be discussed in some detail, including how to estimate some systematic error and nonradiative quenching of the metastable ions. Finally, data will be presented, a final value of the lifetime, including possible systematic errors, will be determined, and a discussion of how the results compare with the former experiment will be given.



## II. THEORETICAL OUTLINE

### 1) The Physics of Many–Electron Atoms (Non–relativistic Theory)

The lifetime of the  $N^+(^5S_2)$  metastable state is determined by the spin–orbit induced electric dipole transition probability between  $^5S_2$  and  $^3P_{1,2}$ . The transition rate for such a decay can be described as

$$A_j = \bar{A} \left| \int \Psi_{f,j} e \vec{r} \Psi_i d\tau \right|^2; \quad j=1,2 \quad (2.1)$$

where  $\bar{A}$  is a constant,  $\Psi_i$ ,  $\Psi_{f,j}$  are the initial and final state functions respectively, and  $e \vec{r}$  is the electric dipole operator.

The radiative lifetime of the initial state, then, is simply

$$\tau_i = 1 / \sum_j A_j \quad (2.2)$$

Therefore, in order to calculate the lifetime of the  $N^+(^5S_2)$ , we need to know the related state wave functions. Those wave functions are the solutions of the Schrödinger equation of the system. But the Schrodinger equation cannot be solved exactly for many–electron atoms so that approximation methods must be used. A detailed treatment of a many–electron system should take into account:

- i)  $H_1$ , the kinetic energy of the electrons and their potential energy in the electrostatic (Coulomb) attractive field of the nucleus (assumed to be point–like and infinitely massive compare with the electron mass).
- ii)  $H_2$ , the electrostatic (Coulomb) repulsion between the electrons.
- iii)  $H_3$ , the magnetic interaction of the electronic spins with their orbital motion (spin–orbit interaction).
- iv)  $H_4$ , several small effects such as spin–spin interactions between the electrons, various relativistic effects, radiative corrections and nuclear corrections (due to the finite mass of the nucleus, its finite extension, nuclear

magnetic dipole moments, etc.).

In other words, the Hamiltonian of the system can be written as

$$H = H_1 + H_2 + H_3 + H_4 \quad (2.3)$$

If  $H_1 \gg H_2 \gg H_3 \gg H_4$ , then perturbation theory could be employed. But for many-electron atoms or ions,  $H_1 \gg H_2$  may not be true. In that case, the central field approximation should be used before perturbation theory can be employed.

We shall first discuss the central field approximation. For simplicity, let us neglect all the "small" effects:  $H_3$  and  $H_4$ . The Hamiltonian of the  $N$ -electron atom (ion) in the absence of external fields can then be written as

$$\begin{aligned} H &= H_1 + H_2 \\ &= \sum_{i=1}^n \left( -\frac{\hbar^2}{2m} \nabla_{\vec{r}_i}^2 - \frac{ze^2}{(4\pi\epsilon_0)r_i} \right) + \sum_{i>j=1}^n \frac{e^2}{(4\pi\epsilon_0)r_{ij}} \end{aligned} \quad (2.4)$$

where  $\vec{r}_i$  denotes the relative coordinate of the electron  $i$  with respect to the nucleus,  $r_{ij} = |\vec{r}_i - \vec{r}_j|$  and the last summation is over all pairs of electrons. It is convenient to use atomic units, where  $m = \hbar = e = 4\pi\epsilon_0 = 1$ . The equation (2.4), then, becomes

$$H = \sum_{i=1}^n \left( -\frac{1}{2} \nabla_{\vec{r}_i}^2 - \frac{z}{r_i} \right) + \sum_{i>j=1}^n \frac{1}{r_{ij}} \quad (2.5)$$

The central field approximation is simply writing the Hamiltonian as follows:

$$H = \overbrace{\sum_{i=1}^n \left( -\frac{1}{2} \nabla_{\vec{r}_i}^2 + V(r_i) \right)}^{H_c} + \overbrace{\sum_{i>j=1}^n \frac{1}{r_{ij}} - \sum_{i=1}^n \left( \frac{z}{r_i} + V(r_i) \right)}^{H'_2} \quad (2.6)$$

where

$$V(r_i) = -\frac{Z}{r_i} + S(r_i) \quad (2.7)$$

and  $\sum_i S(r_i)$  is a large spherically symmetric component of the inter-electron repulsion term  $\sum_{i>j} \frac{1}{r_{ij}}$ . From (2.6) we can see that all we have done is to add and subtract the expression  $\sum_i V(r_i)$  in (2.5). But the perturbation  $H'_2$  defined by (2.6) is much smaller than the term  $H_2 = \sum_{i>j} \frac{1}{r_{ij}}$  representing the full mutual repulsion between the electrons, therefore perturbation theory can be used.

As a zeroth order approximation, we shall begin by neglecting the perturbation  $H'_2$  and concentrate our attention on the central field Hamiltonian  $H_c$  which, as seen from (2.6), contains the kinetic energy  $\sum_i -\frac{1}{2} \nabla_{r_i}^2$ , the potential energy in the field of the nucleus  $\sum_i -\frac{Z}{r_i}$ , and the average (spherical) electron repulsion energy  $\sum_i S(r_i)$ . The corresponding Schrödinger equation then reads

$$H_c \Psi_c = \sum_{i=1}^n \left( -\frac{1}{2} \nabla_{r_i}^2 + V(r_i) \right) \Psi_c = E_c \Psi_c \quad (2.8)$$

where  $\Psi_c$  is the N-electron central field wave function which satisfies the requirements of the Pauli exclusion principle and can be written as

$$\Psi_c(q_1, q_2, \dots, q_n) = \frac{1}{\sqrt{n!}} \begin{vmatrix} \mu_\alpha^{(q_1)} & \mu_\beta^{(q_1)} & \dots & \mu_\gamma^{(q_1)} \\ \mu_\alpha^{(q_2)} & \mu_\beta^{(q_2)} & \dots & \mu_\gamma^{(q_2)} \\ \vdots & \vdots & \ddots & \vdots \\ \mu_\alpha^{(q_n)} & \mu_\beta^{(q_n)} & \dots & \mu_\gamma^{(q_n)} \end{vmatrix} \quad (2.9)$$

where  $q_i$  represents the spatial and spin coordinate and

$$\mu_\gamma^{(q_i)} = \mu_{n l m_l m_s}^{(q_i)} = \mu_{n l m_l}(\vec{r}_i) \chi_{m_s} \quad (2.10)$$

Since  $H_c$  is central and separable to N single-independent Hamiltonian, so the

one-electron or central field orbitals  $\mu_{\nu}(q_i)$  are products of spin orbitals times spatial orbitals, which are products of radial functions times spherical harmonics,

$$\mu_{n l m_l}(\vec{r}_i) = R_{n l}(r_i) Y_{l m_l}(\theta, \varphi) \quad (2.11)$$

where the radial function satisfies the equation

$$-\frac{1}{2} \left( \frac{d^2}{dr_i^2} + \frac{2}{r_i} \frac{d}{dr_i} - \frac{l(l+1)}{r_i^2} \right) R_{n l}(r_i) + V(r_i) R_{n l}(r_i) = E_{n l} R_{n l}(r_i) \quad (2.12)$$

and  $Y_{l m_l}(\theta, \varphi) \chi_{m_s}$  for every electron is known. The total energy  $E_c$  in the central field approximation is the sum of the individual electron energies, namely

$$E_c = \sum_{i=1}^n E_{n_i l_i} \quad (2.13)$$

in which, the energy eigenvalues of each electron,  $E_{n_i l_i}$ , do not depend on the quantum number  $m_l$ , because the potential  $V(r_i)$  in (2.7) is spherically symmetric. However, in contrast to the hydrogenic case, they depend on both  $n$  and  $l$  because  $V(r_i)$  is not simply the Coulomb potential. Higher order approximation can be made through perturbation theory.

A more elaborate approximation for complex atoms (ions) is the Hartree-Fock or self-consistent field method.<sup>35</sup> This is an independent particle model, according to which each electron moves in an effective potential which takes into account the attraction of the nucleus and the average effect of the repulsive interactions due to the other electrons. Each electron in a multielectron system is then described by its own wave function. In accordance with the independent particle approximation and the Pauli exclusion principle, the  $N$ -electron wave function is a Slater determinant  $\Psi$  (same as Eq.(2.9)), or, in other words, an antisymmetric product of individual electron spin-orbitals. The Slater determinant is optimized by using the variational method to determine the 'best' individual electron spin-orbitals.

## 2) Calculations of the $N^+(^5S_2)$ Radiative Lifetime

The  $^5S_2$  state is the first excited state of  $N^+(1s^2 2s\ 2p^3)$  above the terms of the  $(1s^2)2s^2 2p^2$  configuration:  $^3P$ ,  $^1D$ ,  $^1S$ . Direct radiative decay from  $^5S_2$  to those lower energy states can only occur through magnetic quadrupole transitions. However, the decay could also be possible through spin-forbidden electric dipole transitions (intersystem transitions). We can achieve this transition if the initial  $^5S_2$  state is slightly mixed with other  $J = 2$  levels ( $^3D_2$ ,  $^3P_2$ ,  $^1D_2$ ,  $^1P_2$ ) of the  $1s^2 2s\ 2p^3$  configuration through spin-orbit interaction.

Hibbert and Bates<sup>5</sup> proved that the spin-orbit induced electric dipole transitions from  $^5S_2$  to  $^3P_1$  and  $^3P_2$  dominated all others, and that the principal magnetic quadrupole transitions, also to the  $^3P_J$  levels, had probabilities approximately five orders of magnitude smaller. Based on the Hartree-Fock functions of the  $2s^2 2p^2$  and  $2s\ 2p^3$  states made by Roothaan and Kelly,<sup>11</sup> and then by introducing further configurations Hibbert and Bates determined that the lifetime for the  $^5S_2$  is 6.4 ms.

Dalgarno et. al.,<sup>4</sup> on the other hand, estimate a lifetime of 5.8 ms by extrapolation along the isoelectronic sequence. Our experimental result ( $6.4 \pm 0.7$ ms) is in very good agreement with these results.

### III. EXPERIMENTAL FACILITIES

A block diagram for the facility to measure the  $N^+(^5S_2)$  lifetime is shown in Fig.(1). The facility includes a vacuum system, a rf-quadrupole ion trap, an ion creation and detection system, a photon detection and counting system, a timing control system, and a data analysis system.

#### 1) The Vacuum System

The vacuum system produces a background pressure low enough to minimize the influence of impurity ion signals on our experimental results.

As can be seen in Fig.(2), the vacuum chamber consists simply of a main chamber to house the ion trap apparatus, electron gun and CEM, and a flange to which the ion trap apparatus is attached. The entire chamber is pumped by a VHS-4 diffusion pump backed by a mechanical pump. A liquid nitrogen cold trap is placed between the chamber and the diffusion pump to minimize contamination of the vacuum chamber by pump oil. A gate valve with a thermocouple gauge is set in between the diffusion pump and mechanical pump to monitor the background pressure of the system before the diffusion pump can be started.

The vacuum chamber configuration is shown in Fig.(3). The main chamber consists of six ports. The bottom port is connected to the vacuum pump system. The top port is simply sealed (it is not used in this experiment). The right port is connected to the photomultiplier tube with a sapphire window and a filter in between. Two side ports are used for mounting the ion trap apparatus with a feedthrough (on the lower end) and the channel electron multiplier (on the higher end). The alignment between the ion trap and PMT is important for correct photon detection.

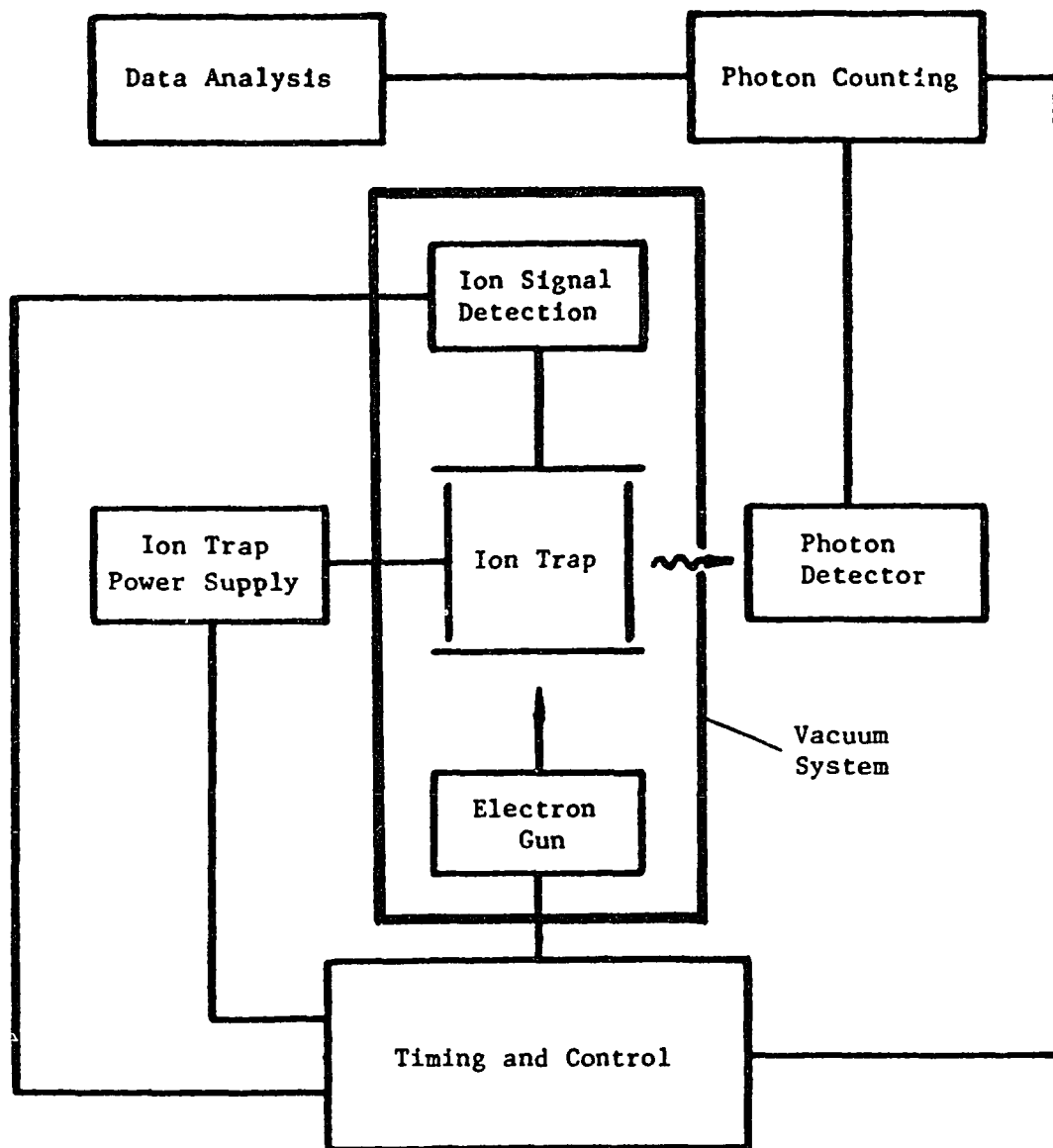


Fig.(1) Block diagram of the  $N^+(^5S_2)$  lifetime experiment.

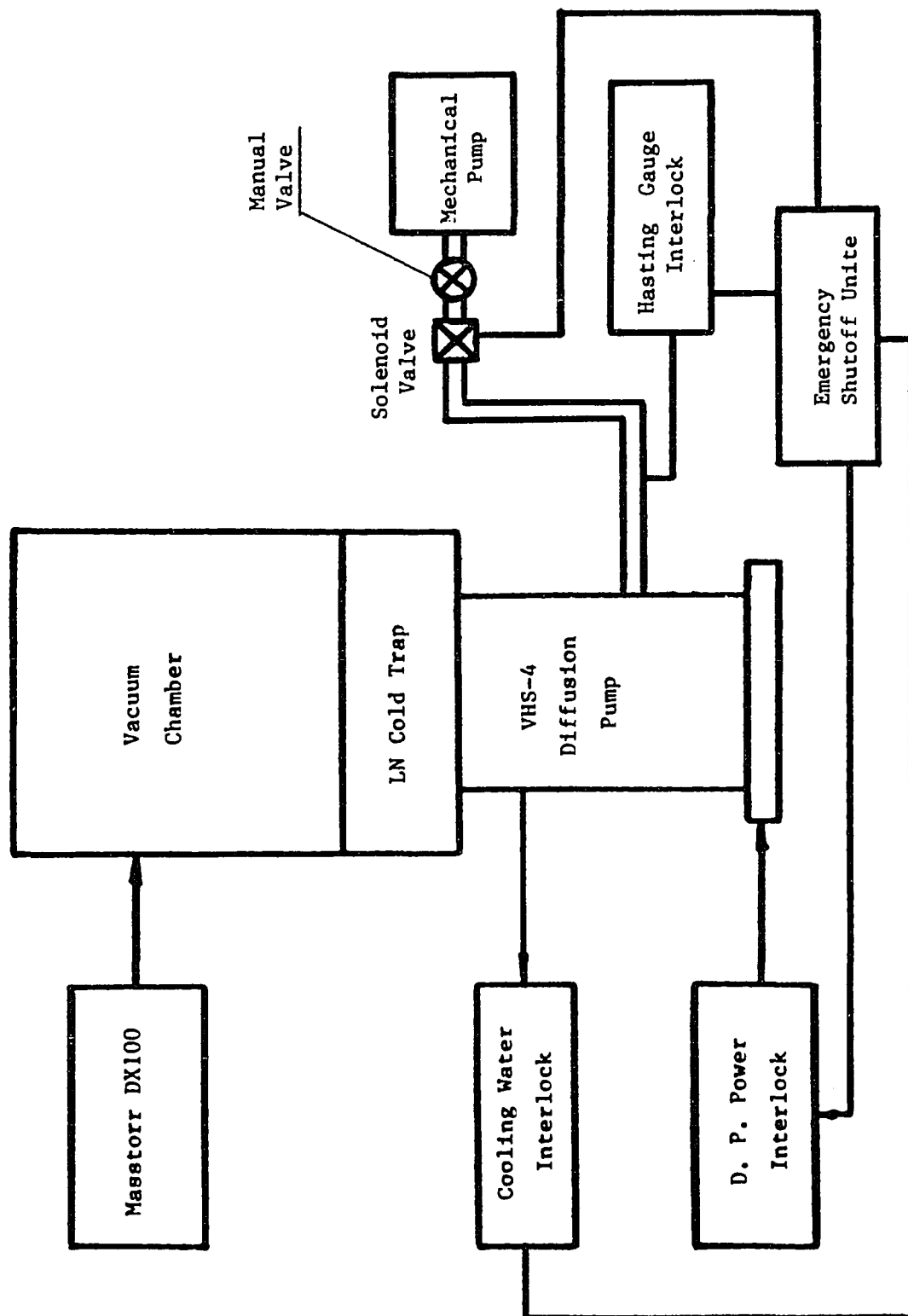


Fig.(2) The Vacuum System.



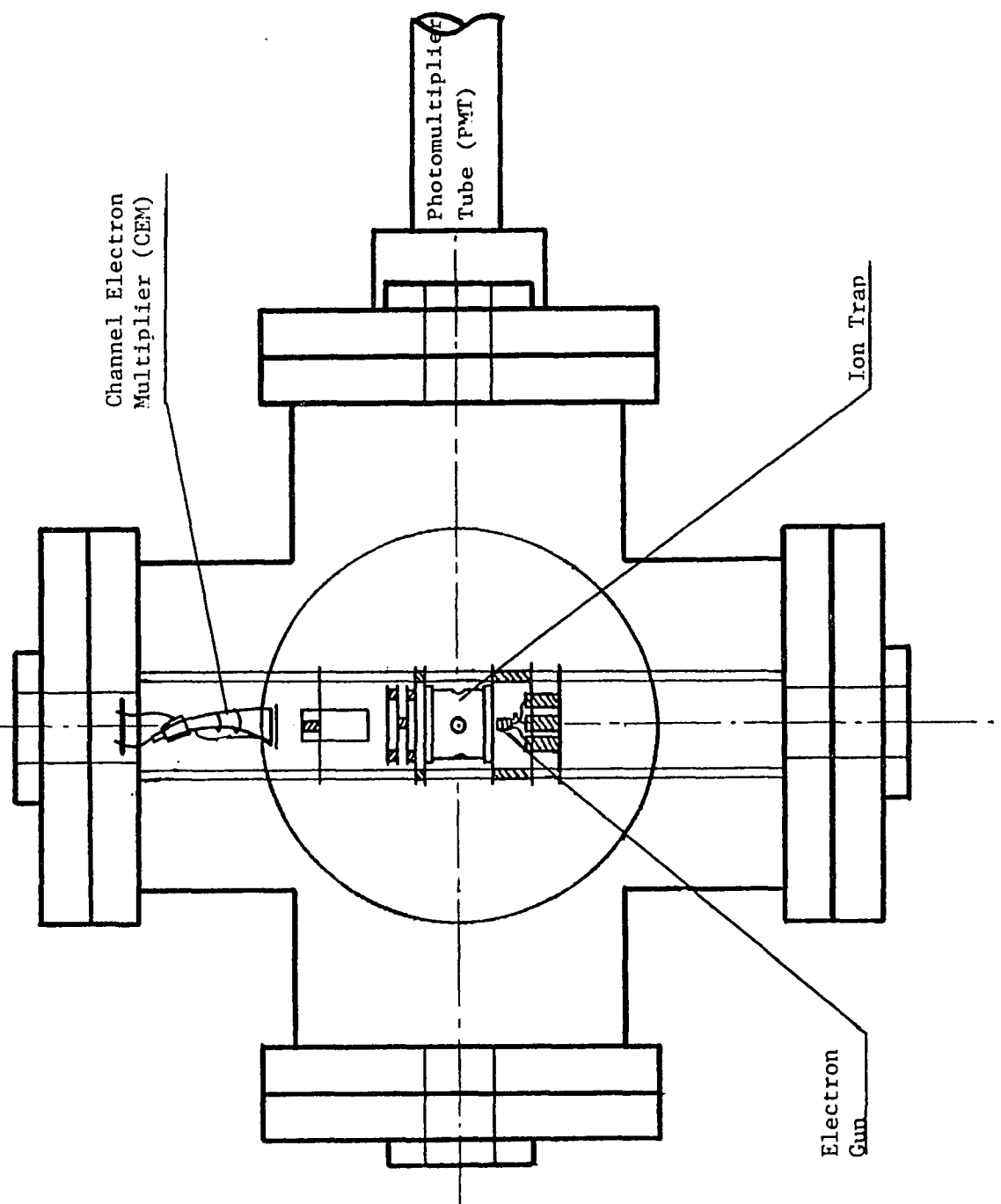


Fig.(3) The Vacuum Chamber Configuration

With this vacuum system, a background pressure of  $5 \times 10^{-9}$  torr can be obtained without baking. The pressure in the vacuum chamber can be measured by a quadrupole mass spectrometer (Masstor DX100)<sup>36</sup> mounted on the left port of the vacuum chamber.

An interlock protection system is used which will turn off the diffusion pump and isolate the vacuum chamber to avoid pump oil from the mechanical pump if:

- i) the power supply is shut off for more than 15 sec.
- ii) the cooling water for diffusion pump runs below an acceptable level.
- iii) unacceptable high pressure (10 mTorr) at the mechanical pump is reached.

## 2) The RF–Quadrupole Ion Trap

The ion trap is the key device for this experiment. It has the ability to confine the desired ions for relatively long time with negligible perturbation during the measurement. The ion trap in this work was made from meshed stainless steel. The configuration of the ion trap used in this work is shown in Fig.(4). The trap is composed of two end electrodes and a ring electrode with small holes cut into the ring electrode to allow better photon detection. The size of this ion trap (see Fig.(5)) is

$$r_0 = z_0 = 1.68 \text{ cm}$$

The quadrupole ion trap was first described by Paul<sup>12</sup> and its feasibility was first demonstrated by Berkling<sup>13</sup> and Fischer.<sup>14</sup> Since that time, many workers have contributed to the development of the quadrupole trap and the study of its properties and characteristics. Most notable among these are Dawson et al.<sup>15, 16, 17, 18, 19, 20, 21, 22</sup> and Todd et al.<sup>19, 23, 24, 25</sup> who carried out extensive investigations on many aspects of the trap. However, the studies mentioned above concentrated on ion traps with hyperbolic electrodes.

In 1973, Benilan and Audoin<sup>26</sup> presented the theoretical description of a

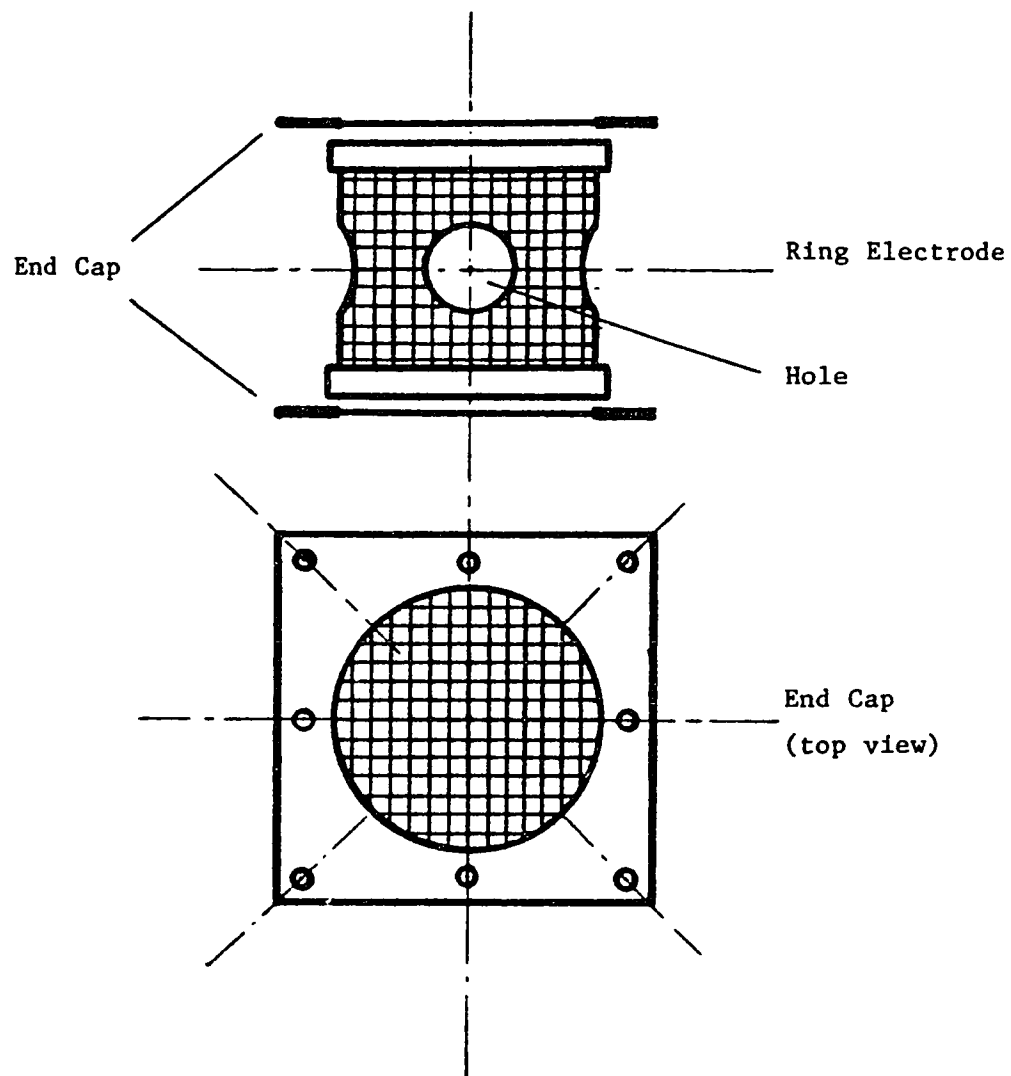


Fig.(4) Configuration of the Ion Trap.

cylindrical ion trap. The cylindrical ion trap was chosen not only because it is easy to machine but because it was felt that the various holes that had to be cut into the trap electrodes would perturb the electric fields to a smaller degree in the cylindrical trap than in the hyperbolic trap.

To understand the performance of the ion trap, a brief outline of ion trap theory is necessary. Detailed discussion of ion traps can be found in many other papers.<sup>27, 28</sup> The trap in this work, as mentioned above, is a cylindrical ion trap. Unlike a hyperbolic trap, there is no simple solution for the potential distribution. However, it has been shown that the potential distribution at and near the center of the cylindrical trap is very close to that of the hyperbolic trap.<sup>26</sup> Furthermore, Knight<sup>29</sup> already gave the general form of the potential distribution, in which the axial size  $z_0$  is independent to the radial size  $r_0$ , and it was well confirmed by our experiments as well as other experiments. Since the ions are confined near the center of the trap, so, for simplicity, the theoretical discription for hyperbolic trap can be used for cylindrical trap. The potential distribution, then, is

$$\phi(r, z) = \frac{U}{r_0^2 + 2z_0^2} \left( r^2 - 2(z^2 - z_0^2) \right) \quad (3.1)$$

where we specified that the two end electrodes are grounded and there is a potential

$$U = U_0 - V_0 \cos \Omega t \quad (3.2)$$

on the ring electrode as shown in Fig.(5). When a charged ion is in this potential it will see a electric field given by

$$\mathbf{E} = -\nabla \phi(r, z) \quad (3.3)$$

and a force

$$\mathbf{F} = e \mathbf{E} = m \ddot{\mathbf{r}} \quad (3.4)$$

acting on it. So the equations of motion for a mass  $m$  with charge  $e$  become:

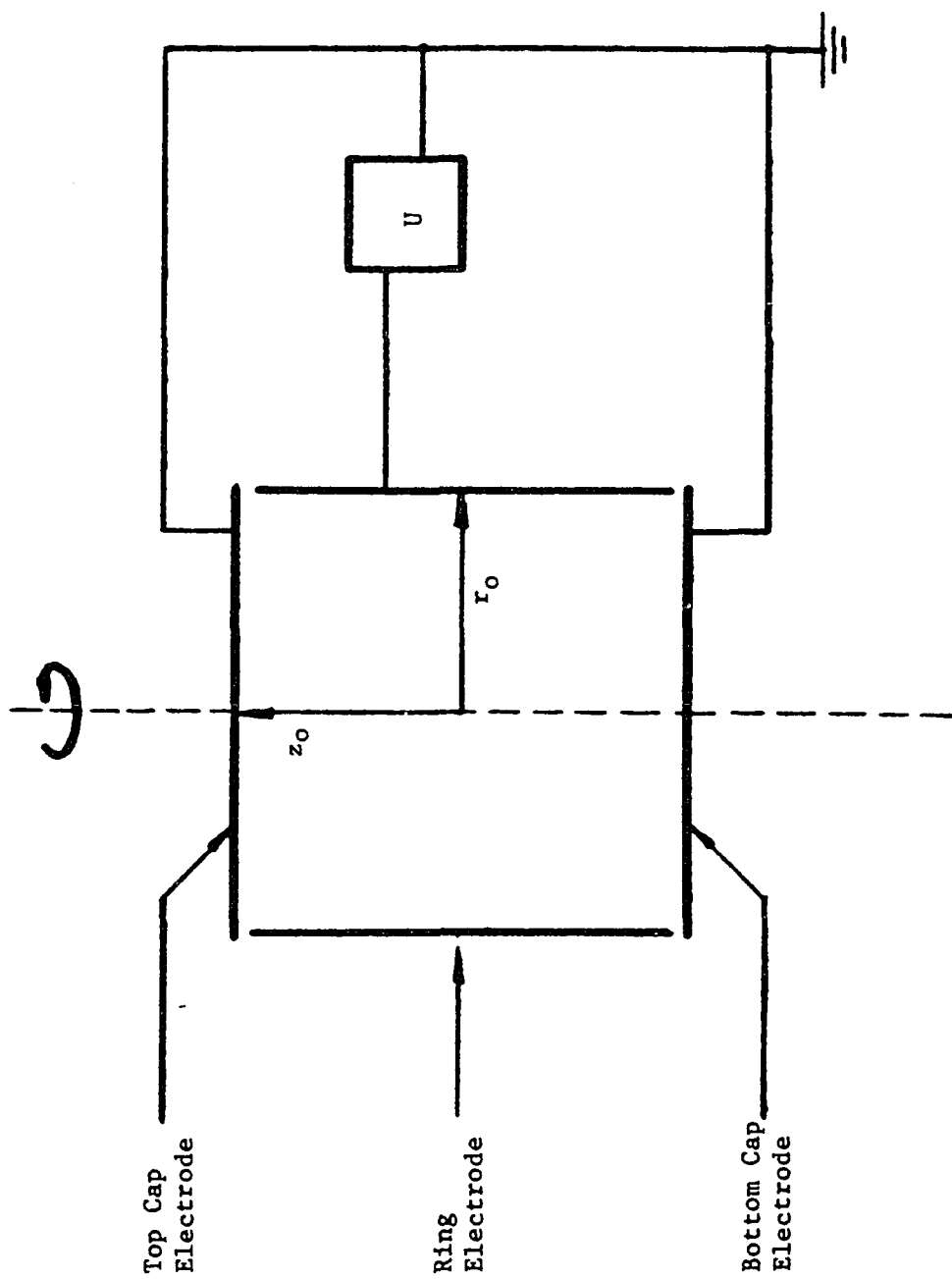


Fig.(5) Geometry of the Cylindrical RF-Quadrupole Ion Trap

$$\ddot{r} = - \left( \frac{e}{m} \frac{2U_o}{r_o^2 + 2z_o^2} \right) r + \left( \frac{e}{m} \frac{2V_o}{r_o^2 + 2z_o^2} \right) r \cos\Omega t \quad (3.5)$$

$$\ddot{z} = \left( \frac{e}{m} \frac{4U_o}{r_o^2 + 2z_o^2} \right) z - \left( \frac{e}{m} \frac{4V_o}{r_o^2 + 2z_o^2} \right) z \cos\Omega t \quad (3.6)$$

If we define:

$$2a_r = -a_z = \frac{16eU_o}{m(r_o^2 + 2z_o^2)\Omega^2} \quad (3.7)$$

$$2q_r = -q_z = \frac{8eV_o}{m(r_o^2 + 2z_o^2)\Omega^2} \quad (3.8)$$

and

$$v = \frac{\Omega t}{2} \quad (3.9)$$

then both  $r$  and  $z$  equations of motion are of the form

$$\frac{d^2u}{dv^2} + (a - 2q\cos 2v) u = 0 \quad (3.10)$$

This is the Mathieu equation. A class of solution, depending on two parameters  $a$  and  $q$ , leads to finite amplitude of the ion motion, i.e., to confinement. Fig.(6) shows the stability diagram obtained by requiring the values of  $a_z$ ,  $a_r$ ,  $q_z$ , and  $q_r$  to be such that the motion is stable in both the axial and radial directions. For an ion of fixed  $\frac{e}{m}$ , selection of the trap voltages and frequency ( $U_o$ ,  $V_o$ , and  $\Omega$ ) can locate the operating point on this diagram. Only if the operating point specified by  $a$  and  $q$  is in the interior of the closed region of Fig.(6) can trapping occur. An approximate solution to the equation of motion, valid for  $q \leq 0.4$  and  $a \ll q$  can be obtained by dividing the motion into two components,<sup>30</sup> a displacement,  $\delta$ , due to the micromotion resulting from the high frequency field and a larger displacement,  $\bar{u}$ , which describes the extent of the motion averaged over a period of the rf drive potential, namely:

$$u = \bar{u} + \delta \quad (3.11)$$

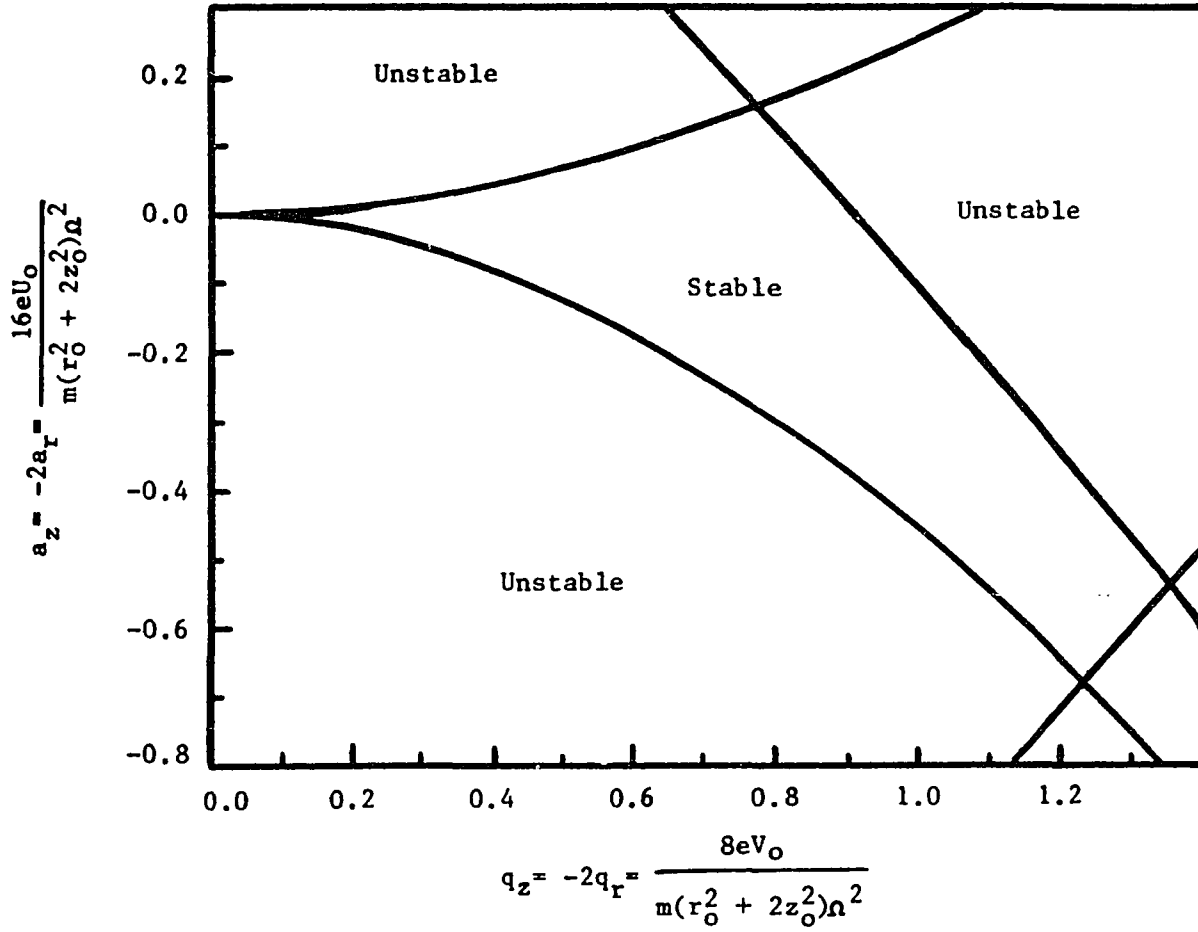


Fig.(6) Stability diagram of the ion trap

where  $\delta \ll \bar{u}$  but  $\frac{d\delta}{dv} \gg \frac{d\bar{u}}{dv}$ .

Then Mathieu's equation becomes

$$\frac{d^2}{dv^2} (\bar{u} + \delta) + (a - 2q \cos 2v) \bar{u} = 0 \quad (3.12)$$

or

$$\frac{d^2 \delta}{dv^2} = - (a - 2q \cos 2v) \bar{u} \quad (3.13)$$

Since  $a \ll q$  and  $\bar{u}$  changes slowly, integration of the above equation gives

$$\delta = - \frac{q\bar{u}}{2} \cos 2v \quad (3.14)$$

and

$$u = \bar{u} + \delta = \bar{u} - \frac{q\bar{u}}{2} \cos 2v \quad (3.15)$$

Substitute this into the original Mathieu equation, we have

$$\frac{d^2 u}{dv^2} = -a\bar{u} + \frac{aq\bar{u}}{2} \cos 2v + 2q\bar{u} \cos 2v - q^2\bar{u} \cos^2 2v \quad (3.16)$$

Averaging over one cycle of the drive frequency gives the equation for the slow macromotion (since the fast motion due to rf drive averaged over a period of the rf drive is equal to zero.)

$$\frac{d^2 \bar{u}}{dv^2} + (a + \frac{q^2}{2}) \bar{u} = 0 \quad (3.17)$$

which, written in terms of time, becomes

$$\frac{d^2 \bar{u}}{dt^2} + (a + \frac{q^2}{2}) \frac{\Omega^2}{4} \bar{u} = 0 \quad (3.18)$$

This equation corresponds to simple harmonic motion with the oscillation frequency

$$\omega = \frac{\Omega}{2} \sqrt{a + \frac{q^2}{2}} \ll \Omega \quad (3.19)$$

$$\bar{u} = A \cos \omega t \quad (3.20)$$

and

$$u = \bar{u} + \delta = A \cos \omega t \left( 1 - \frac{q}{2} \cos \Omega t \right) \quad (3.21)$$



A reasonable way to picture the ion motion, then, is a slow harmonic motion at frequency  $\omega$  upon which is superimposed a micromotion at the drive frequency  $\Omega$ . Note that the spectrum of the motion contains components at frequency  $\omega$  as well as  $\Omega \pm \omega$ , which arise from the  $\cos\omega t \cos\Omega t$  term.

The force (averaged over one cycle of drive frequency) on an ion of mass  $m$  and charge  $e$  is therefore given by

$$m \frac{d^2 \bar{u}}{dt^2} = -m \left( a + \frac{q^2}{2} \right) \frac{\Omega^2 \bar{u}}{4} = -e \frac{d\bar{D}}{du} \quad (3.22)$$

For the motion along  $z$  direction:

$$\begin{aligned} \frac{d\bar{D}_z}{dz} &= \frac{m}{e} \left( a_z + \frac{q_z^2}{2} \right) \frac{\Omega^2 z}{4} \\ &= \left( \frac{-4U_o}{(r_o^2 + 2z_o^2)} + \frac{8eV_o^2}{m(r_o^2 + 2z_o^2)\Omega^2} \right) z \end{aligned} \quad (3.23)$$

$$D_z = \left( \frac{4eV_o^2}{m(r_o^2 + 2z_o^2)\Omega^2} - \frac{2U_o}{(r_o^2 + 2z_o^2)} \right) z_o^2 \quad (3.24)$$

similarly, for the  $r$  motion we have

$$D_r = \left( \frac{eV_o^2}{m(r_o^2 + 2z_o^2)\Omega^2} + \frac{U_o}{(r_o^2 + 2z_o^2)} \right) r_o^2 \quad (3.25)$$

where  $D_r$  and  $D_z$  are defined as potential well depths in the radial and axial directions.

The total effective potential seen by an ion, then, can be written as

$$\phi_{\text{eff}} = D_r \frac{r^2}{r_o^2} + D_z \frac{z^2}{z_o^2} \quad (3.26)$$

to make  $\phi_{\text{eff}} = 0$  at the trap center.

In the case of a spherical well, we have  $D_r = D_z = D$ . For our trap design  $r_o = z_o$ . We can get

$$D = \frac{2}{3} U_o \quad (3.27)$$

which shows that the spherical potential well depth is directly proportional to the DC bias of the ion trap.

The optimum trapping parameters have been investigated both theoretically and experimentally.<sup>31, 32</sup> The results, plotted on the stability diagram in Fig.(7), are in good agreement with each other. They are also in good agreement with the data obtained by our trap. For a fixed  $q_z$  (or  $a_z$ ), the value of  $a_z$  (or  $q_z$ ) which results in a spherical potential well will give maximum stability.

### 3) Electron Gun and Channel Electron Multiplier

The ion creation and detection system in this experiment includes an electron gun and a channel electron multiplier.

#### A. Electron Gun

The electron gun used was a 7mm long, 3mm diameter tungsten dispenser cathode, which was made from porous tungsten with a formula of barium oxide dispersed throughout the matrix. This dispenser cathode will allow higher emission current densities at lower operating temperature with decreased sublimation rates and greater resistance to poisoning from the cathode environment.

The electron gun was screw fixed to a stainless steel support and mounted 2mm from the lower end cap of the ion trap [Fig.(3)]. The cathode was heated by  $I \simeq 0.8A$ , 60Hz current with the potential difference of 4.0V across it during the experiment. In order to generate  $N^+(^5S_2)$  from background  $N_2$  gas through electron impact with molecular nitrogen, bias voltage of  $-200V$  was set to the electron gun whereas the lower end cap of the ion trap was grounded. Under these circumstances

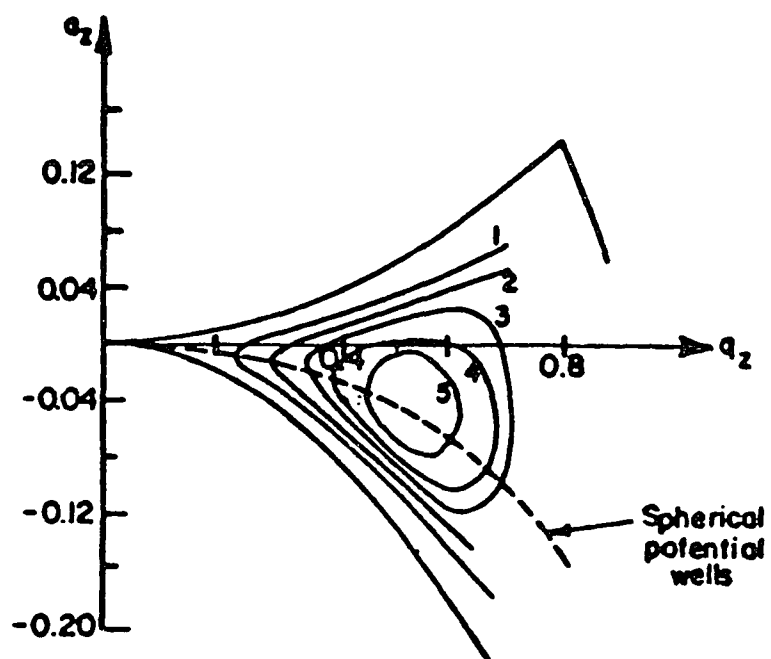


Fig.(7) Contours of the number of ions stored  
(from Reference 28)

the electrons produced by the electron gun are accelerated into the ion trap and bombard the molecular nitrogen there. Alternatively, the electrons can be confined to the region around the electron gun by adding a positive bias of +100v to the electron gun. This prevents the unwanted electrons getting into the ion trap to disturb the lifetime measurement.

#### B. Channel Electron Multiplier (CEM)

The model 4716 high current CEM has been used to detect the ions confined in the ion trap. The observation takes place during the electron gun "off" time. A negative high voltage pulse ( $-70\text{v}$ ) was applied to the higher end cap electrode of the trap nearest to the CEM so that the ions confined in the ion trap were driven out through this electrode, and into the CEM, as seen in Fig.(3). The ion signal was amplified by means of secondary electron emission in the CEM, and then displayed on an oscilloscope. We confirmed that the signals could be ascribed to  $\text{N}^+$  or  $\text{N}_2^+$  since they vanished if either the  $\text{N}_2$  was removed or the ion trap was detuned to prevent their storage. Time of flight technique has also been used to confirm  $\text{N}^+$  storage.

#### 4) The Photon Detection System

The photon detection system consists of i) a sapphire window to allow UV photons to pass through. ii) an interference filter, which transmits 21.6% at a wavelength of  $2150 \text{ \AA}$  with a bandwidth of  $230 \text{ \AA}$ , to attenuate blackbody radiation from the hot electron gun cathode. iii) a Photomultiplier Tube (PMT) to detect photons, and iv) a Multi-Channel-Analyzer (MCA), which serves as a photon counter. These are shown schematically in Fig.(8).

The PMT converts the incident radiation into electrical signals by use of the phenomenon of photoemission and then amplifies the signals by means of secondary emission.

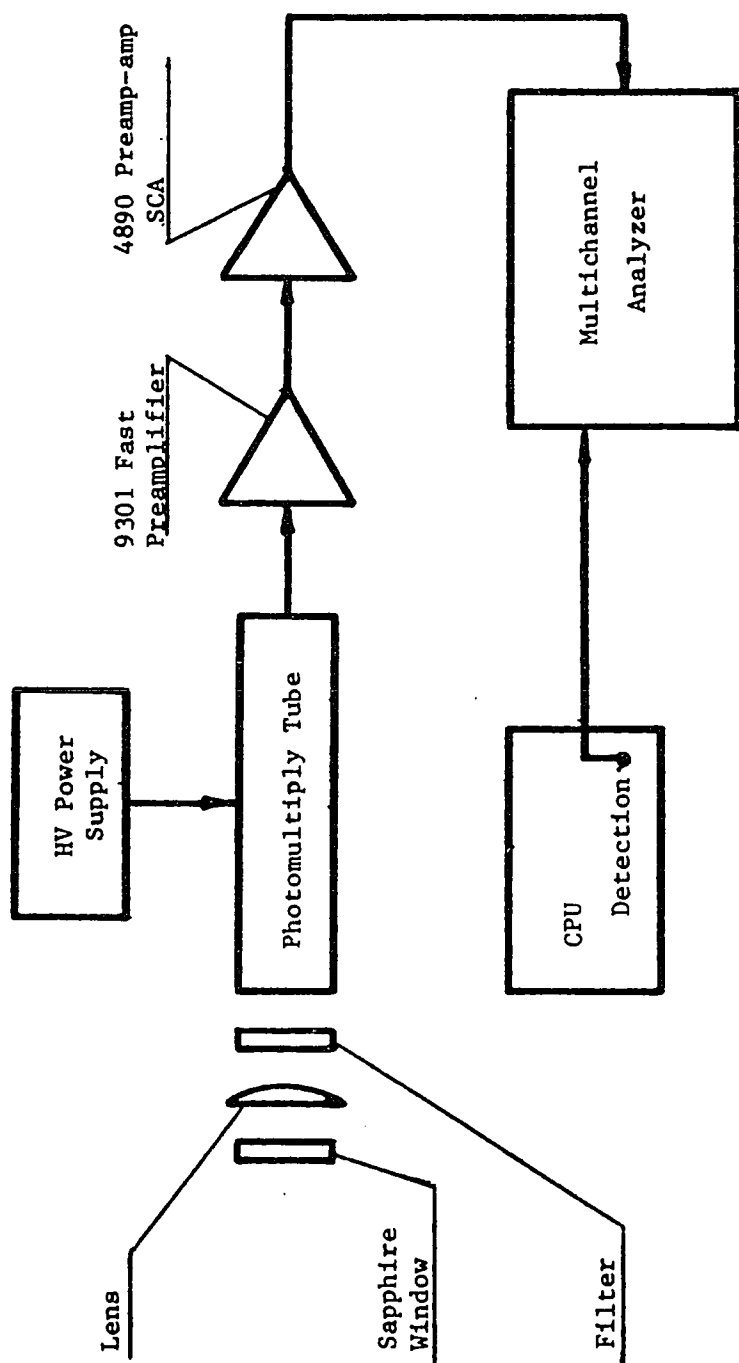


Fig.(8) Photon Detection System

The PMT used in this work is the EMR Model 541Q-05M-13 multiplier phototube, which is an end-on tube with a 25mm effective diameter, semitransparent, solar blind photocathode. Its window material is selected ultraviolet grade sapphire ( $\text{Al}_2\text{O}_3$ ). The spectral sensitivity is characterized by high ultraviolet sensitivity with an extremely sharp cut off of atmosphere-penetrating solar radiation. As shown in Fig.(9), the short wavelength cut off is at  $1700\text{\AA}$  and the longer wavelength response is extended out to  $3650\text{\AA}$  with quantum efficiency of 0.001%. Peak sensitivity occurs near  $2537\text{\AA}$ . Typical voltages of 2100v to 2600v are required for current amplifications of  $10^6$  to  $10^7$ .

The output pulses from the PMT are amplified by a 9301 ORTEC Fast Amplifier., passed through a discriminator (ORTEC 4890 Pre-Amp SCA) and routed to a scaler (MCA) which is gated on by the falling edge of the CPU relaxation pulse. The pulse amplification gain is set to give saturating pulses at a moderate high voltage and the discriminator is set higher than the amplifier noise level. The MCA performs in MCS (Multichannel Scaling) mode, which is a time sweep of the channels in the MCA with each channel being an equal time interval to total sweep. During each channel time interval, the memory location for that channel counts digital pulses at random rates up to 10 MHz. Thus, the resulting display is a frequency histogram with time as the horizontal axis. The dwell time ranges from  $10\text{ }\mu\text{s}$  through 1 second.

The data received by the MCA can either be displayed on a built-in Cathode-Ray Tube (CRT) or stored in the non-volatile memory. The stored data can be recalled when desired.

## 5) Control Process Unit (CPU)—the Experimental Timing Control Box

In the previous sections, the various functions and measurements which make up the experiment were discussed separately. An understanding of how these pieces

# SPECTRAL RESPONSE

26

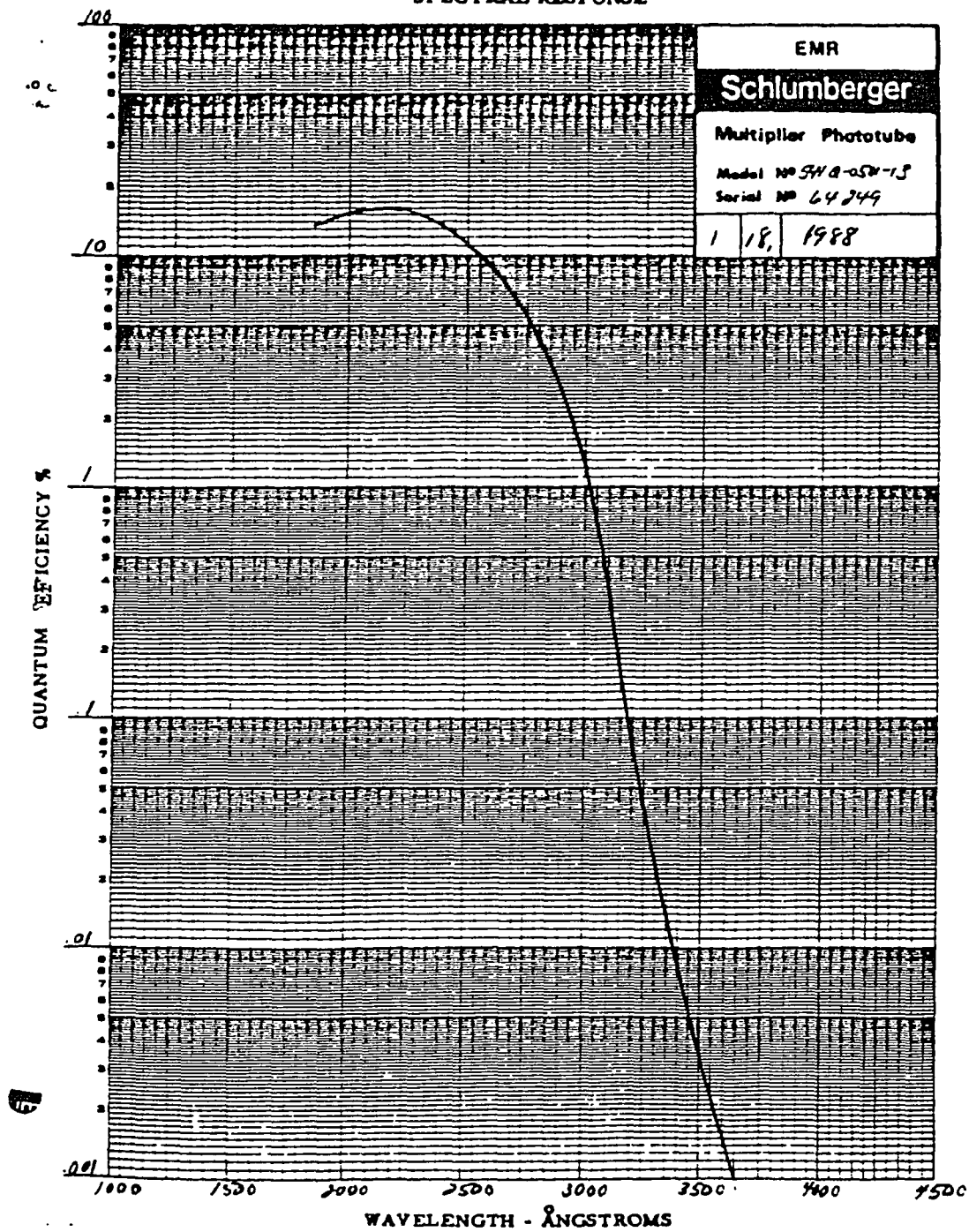


Fig.(9) The Photomultiplier Tube spectral response.

are integrated to form the whole experiment is best accomplished by describing the experimental timing control box (CPU).

The CPU contains logic circuitry which generates 4 TTL logic pulses. The first pulse controls the electron gun "on" time (the ionization period). The trailing edge of the first pulse triggers the second pulse, the relaxation pulse. The length of the relaxation pulse determines the waiting period between electron gun shut off and the detection pulse. The third pulse, the detection pulse, is turned on by the falling edge of the relaxation pulse. The leading edge of this pulse turns on the CEM. The measurement is allowed after an appropriate relaxation time and before the next electron gun "on" pulse. The fourth pulse, triggered by the trailing edge of the detection pulse, will dump the ions out from ion trap to the CEM. The dump pulse and the CEM are used only to identify the ions confined in the ion trap. This will help to select appropriate parameters for the ion trap to confine the desired ion. During the  $N^+(^5S_2)$  radiative lifetime measurement, the MCA is gated on by the leading edge of the detection pulse to gather the data, whereas the CEM and the dump pulse are not used to avoid the disturbance of ion storage. The MCA sweep time duration has to be longer than the CPU detection pulse width, otherwise the MCA sweep signal will turn on automatically and start to sweep again if the CPU detection pulse is still high. On the other hand, the MCA sweep should turn off before the next e gun pulse for the same reason.

## 6) Data Analysis System

Data analysis was done by using the "DISCRETE" program.<sup>33</sup> It is a FORTRAN IV program for the automatic analysis of data being represented by:

$$N_k = \sum_{j=1}^m \alpha_j \exp(-\lambda_j t_k), \quad k = 1, 2, \dots, N, \quad m \leq 9$$

A provision can be made for an unknown baseline component  $\alpha_0$  with



$\lambda_0 = 0$ . It is completely automatic in that only the raw data(i.e., the  $N_k$  and  $t_k$ ) are input; no potentially biased initial guesses at the  $\alpha_j$ ,  $\lambda_j$  or  $m$  are needed or even allowed. So the results from this data analysis should be more reliable.

## IV EXPERIMENTAL METHODS AND PROCEDURES

### 1) Experimental Method and General Procedures

The method used to measure the  $N^+ {}^5S_2$  state lifetime was simply to detect spontaneously emitted photons as a function of time.

A single exponential decay signal can be characterized by

$$N(t) = N_o \exp(-t/\tau) \quad (4.1)$$

and the decay rate at any instant of time  $t$  is defined by

$$\frac{1}{\tau} = -\frac{d}{dt} \left( \ln N(t) \right) \quad (4.2)$$

substituting (4.1) into (4.2), we have

$$\ln N(t) = \ln N_o - \frac{1}{\tau} t \quad (4.3)$$

So the graph of  $\ln N(t)$  vs  $t$  is a straight line with slope  $-\frac{1}{\tau}$  independent of  $t$ , and  $\tau$  is the radiative lifetime. Experimentally we have two steps to complete before the lifetime measurement. First of all, we have to create enough  $N^+({}^5S_2)$  ions, but when we create  $N^+$  we create other kinds of ions as well. So the second step is to select those desired ions and store those ions in a disturbance free area for a time which is much longer than the expected lifetime. Here disturbance free means the disturbance from the surroundings (e.g. the ion trap's RF field) are negligible compared with the interaction between nucleus and electrons of the ion. The third step, then, is simply to detect the spontaneous emission while the ions are in storage. The final step is data analysis. In this experiment, the first three steps were controlled by CPU TTL signals with the typical timing sequence performed by CPU as shown in Fig.(10). The data analysis was performed later by "DISCRETE" computer program. The procedures, described in some detail, are following.

### 2) Creation of $N^+$

$N^+$  ions, in both metastable and ground states, were created in the ion trap

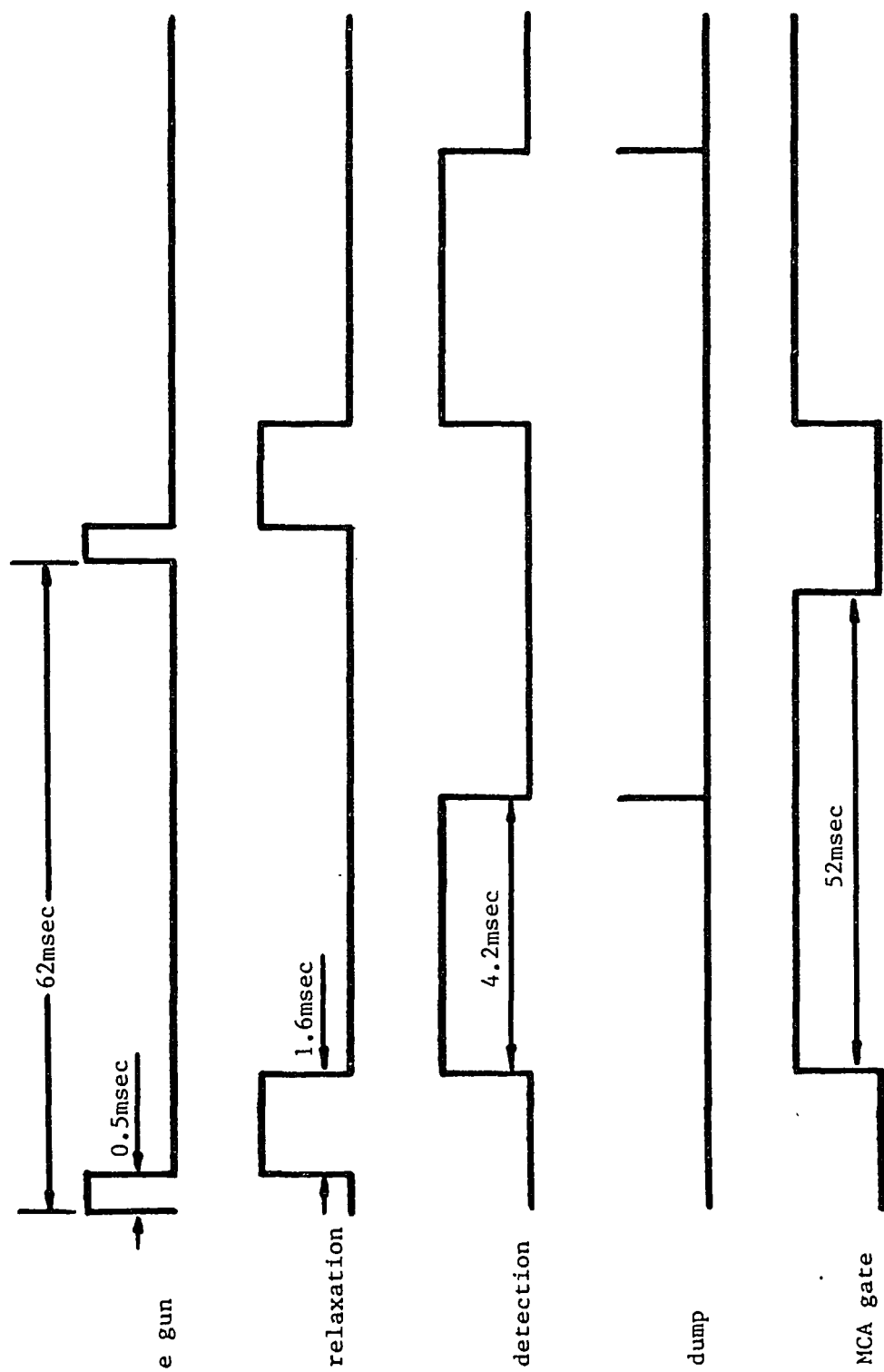


Fig.(10) Experimental timing and control signals

due to the electron impact dissociation and ionization of  $N_2$  gas. The process can be described as



where the effective threshold to produce  $N^+(^5S_2)$  is 37eV.<sup>4</sup> The kinetic energy of the electrons, before impact with  $N_2$ , is determined by the negative bias between the e gun and the end cap of ion trap plus the rf potential field in the ion trap. This initial electron kinetic energy can determine the rates for creation of  $N^+(^5S_2)$  from a certain  $N_2$  back pressure. We estimated those rates by monitoring the 2140Å photon signal while we scanned the negative bias and finally set the bias at -200V. The electron energies under the trap RF power of  $V_o = 400V$ ,  $f_o = 1.2MHz$ , then, can be estimated to be under 500eV. In this energy range, the cross section of producing  $N^+(^5S_2)$  via electron impact on  $N_2$  has been estimated as  $\geq 1 \times 10^{-18}cm^2$ .<sup>3, 4</sup> Time of flight measurements of ion velocities following dissociative ionization of  $N_2$  suggest that  $N^+(^5S_2)$  is formed with an initial kinetic energy around 3eV.<sup>8, 34</sup>

The electron gun negative and positive bias, as mentioned in section III, were supplied by a dual regulated power supply. The switching time (from -200V to +100V) was controlled by the CPU e gun signal. The e gun "on" time (for which -200V was set between electron gun and the end cap of ion trap) was long enough to produce a number of  $N^+(^5S_2)$  ions in the ion trap. To determine the number of  $N^+(^5S_2)$  ions produced in time T, the following equation is used:

$$N = I\sigma n l T \quad (4.5)$$

where I is the electron beam current, n is the neutral parent gas number density,  $\sigma$  is the ionization cross section, l is the path length of the electrons, and T is the electron gun "on" time. In this experiment:

$$I \sim 5A = 5 \times 10^5 \times 6.2 \times 10^{13}e/sec = 3 \times 10^{19}e/sec$$

as tested by Kwong (1981)<sup>9</sup>

$$n \sim 10^{-6} \text{Torr} \times \frac{2.69 \times 10^{19}}{760} = 3.54 \times 10^{10} / \text{cm}^3$$

$$\sigma \sim 10^{-18} \text{cm}^2$$

$$l \sim 2 \text{ cm}$$

and in this experiment we choose  $T = 0.5 \text{ms} = 5 \times 10^{-4} \text{sec}$ . The number of ions produced, then, is

$$N \sim 10^9$$

This number is much greater than the number of ions ( $\sim 10^5$ ) that could be confined in our ion trap due to space charge effects.

The CPU electron gun signal and relaxation signals, combined with the dual regulated power supply's response signal are shown in Fig.(11). From there we can see that the power supply's response signal has a significant rise time ( $\approx 1.2 \text{ms}$ ). Although the electron gun control pulse has already turned off, some energetic electrons still can get into the ion trap to create some "noise" during this period of time. Increasing the positive bias can decrease the rise time. The relaxation signal has been extended such that the relaxation time is greater than the rise time +  $0.3 \text{ms}$  (which is the fast decay time attributed to emission in the  $\text{N}_2$  Lyman–Birge–Hopfield bands<sup>3</sup>).

In order to avoid unexpected disturbances, the vacuum was kept very high ( $0.5 \times 10^{-8} \text{Torr}$ ) before filling the  $\text{N}_2$  gas. The composition of residual gas at background pressure  $5 \times 10^{-9} \text{Torr}$  in the vacuum chamber is shown in Fig.(12). It includes  $\text{H}$ ,  $\text{H}_2$ ,  $\text{HO}$ ,  $\text{H}_2\text{O}$ ,  $\text{CO}$ ,  $\text{CO}_2$ , etc. A background run was made without fill  $\text{N}_2$ , whereas the other parameters were all set the same as those for the  $\text{N}^+(\text{}^5\text{S}_2)$  lifetime measurement. The PMT did not see any decay under this circumstance. That means that the radiation from the residual gas is negligible. Ultrahigh purity  $\text{N}_2$  gas (99.9999%) was used as a parent gas for creation of  $\text{N}^+$ .

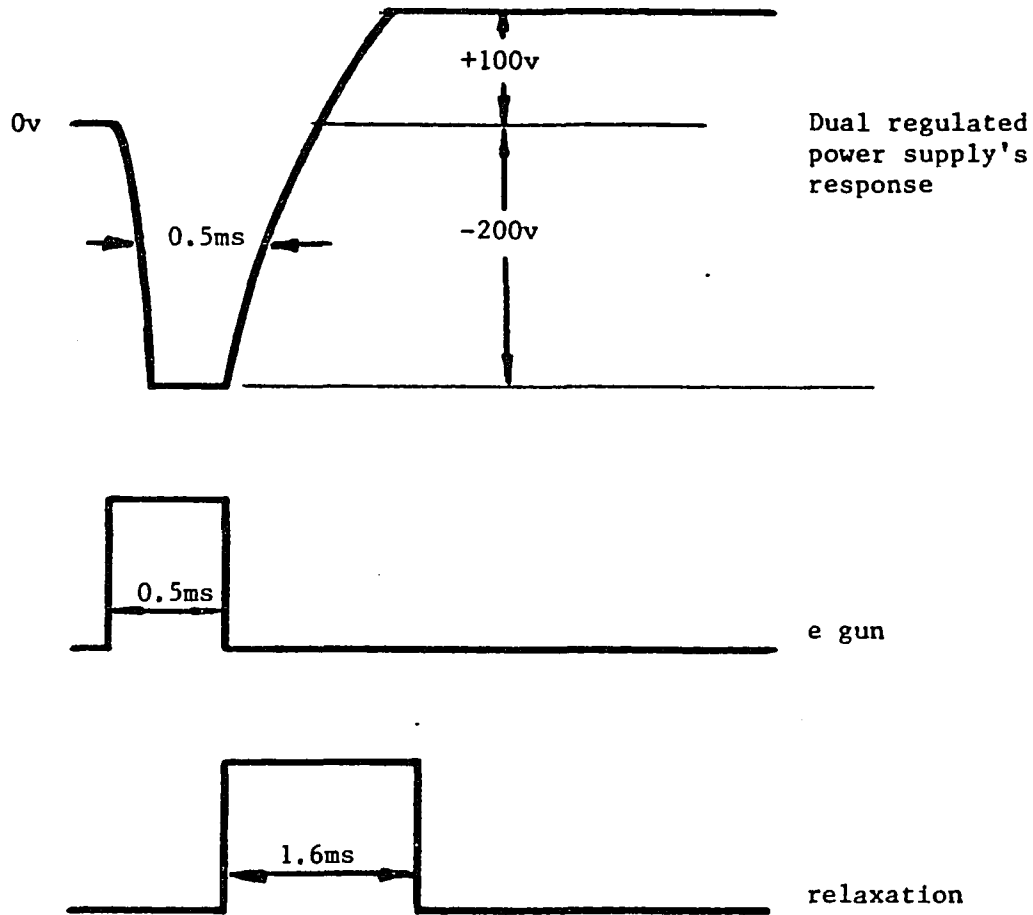


Fig.(11) The CPU e gun signal, relaxation signal combined with the dual regulated power supply's response signal

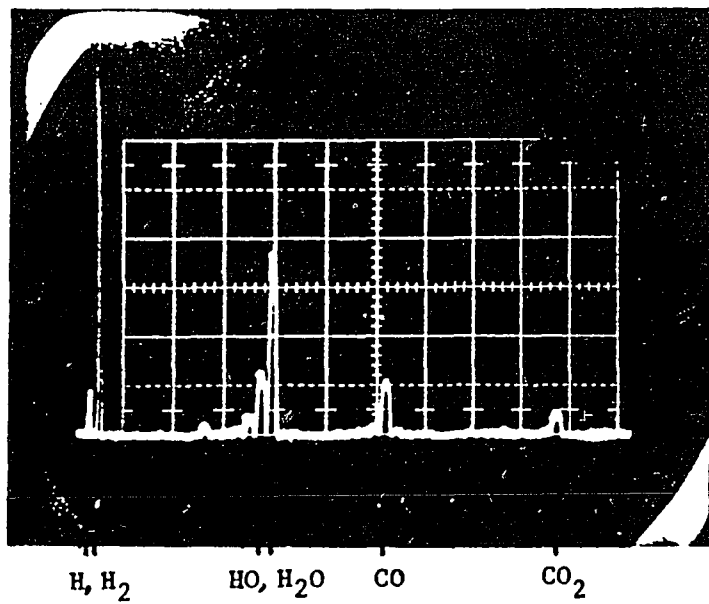


Fig.(12) The residual gas composition

### 3) Ion Selection and Storage

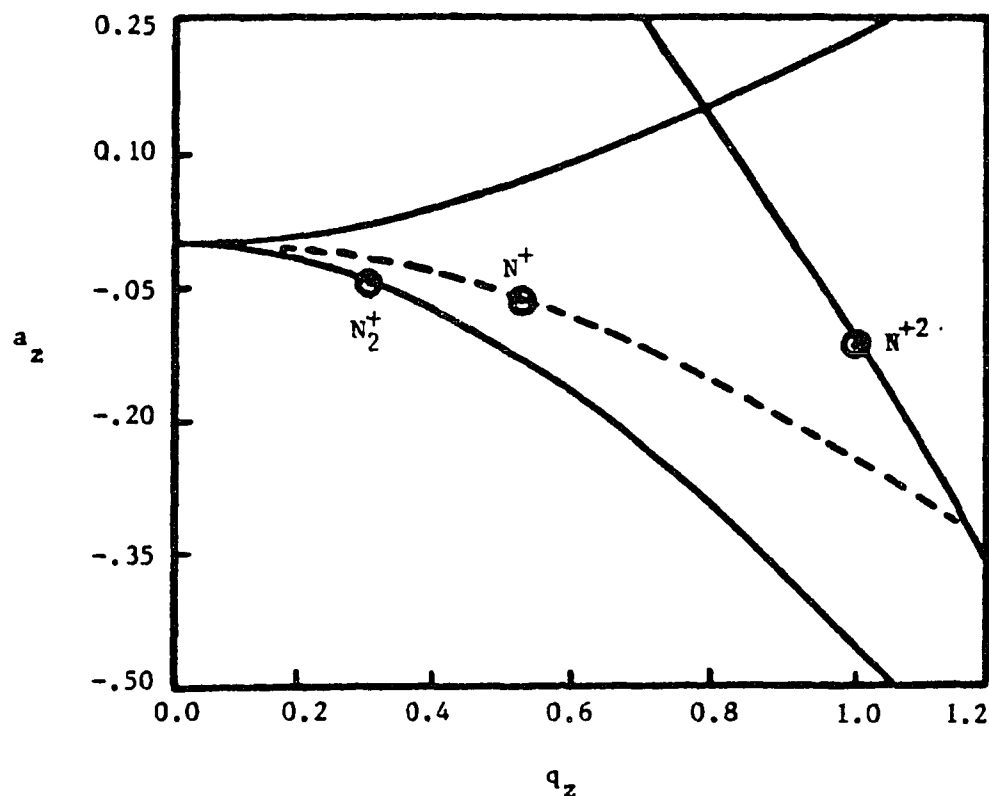
Ions created via electron impact with  $N_2$  could be in many different states. It is very important to exclude the ions other than  $N^+$  from storage and to confine only  $N^+$  ions in a perturbation-free environment for times much longer than the expected radiative lifetime of a few milliseconds. In the last chapter, we saw that the rf quadrupole trap is an ideal tool to do this job.

Calculations locating various ion density peaks on the stability diagram were made. The results showed that:

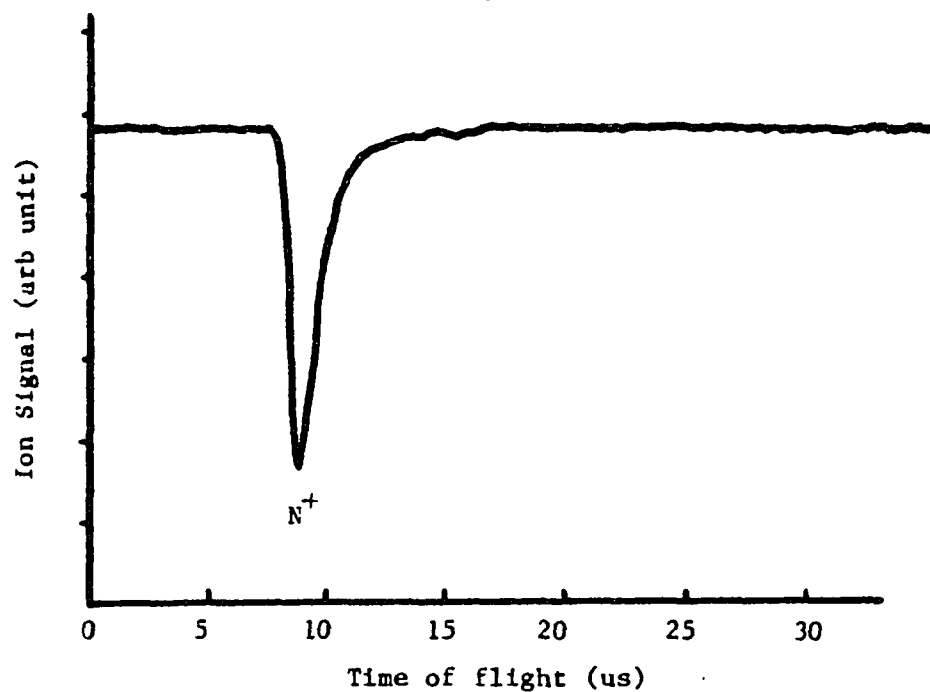
- i) at  $V_o = 400V$ ,  $f_o = 1.2MHz$ ,  $U_o = 25V$ ;  $N^+$  ions sit right on the spherical potential well line (see Fig.(13 a)) and at the largest density area, where  $q_z \sim 0.5$ ,  $a_z \sim -0.04$ . This will give the maximum stability and largest ion density for  $N^+$  confinement. On the other hand,  $N_2^+$  and  $N^{+2}$  can not be confined under this condition.
- ii) at  $V_o = 255V$ ,  $f_o = .65MHz$ ,  $U_o = 20V$ ; only  $N_2^+$  can be trapped. (see Fig.(14 a))
- iii) at  $V_o = 220V$ ,  $f_o = .65MHz$ ,  $U_o = 20V$ ; both  $N^+$  and  $N_2^+$  can be confined. (see Fig.(15 a))

These results are for a trap with ideal hyperbolic electrodes. However, the potential surfaces of a cylindrical ion trap near the center of the trap are very close to the ideal one, as mentioned in the last chapter. To test the system, the ion trap voltages and frequencies have been set at the values as mentioned in i), ii), iii) above respectively. A dump pulse of  $-70V$ , which was gated on by the falling of the detection pulse, has been applied to one of the trap's end caps. This dump pulse will drive ions out the trap to be detected by a channel electron multiplier (CEM), which is gated on by the detection pulse (leading edge). Ion signals are shown in Fig.(13 b), Fig.(14 b), and Fig.(15 b) respectively. Using the time-of-flight technique we can easily identify  $N^+$  and  $N_2^+$ . The time of flight  $t$  is given by the





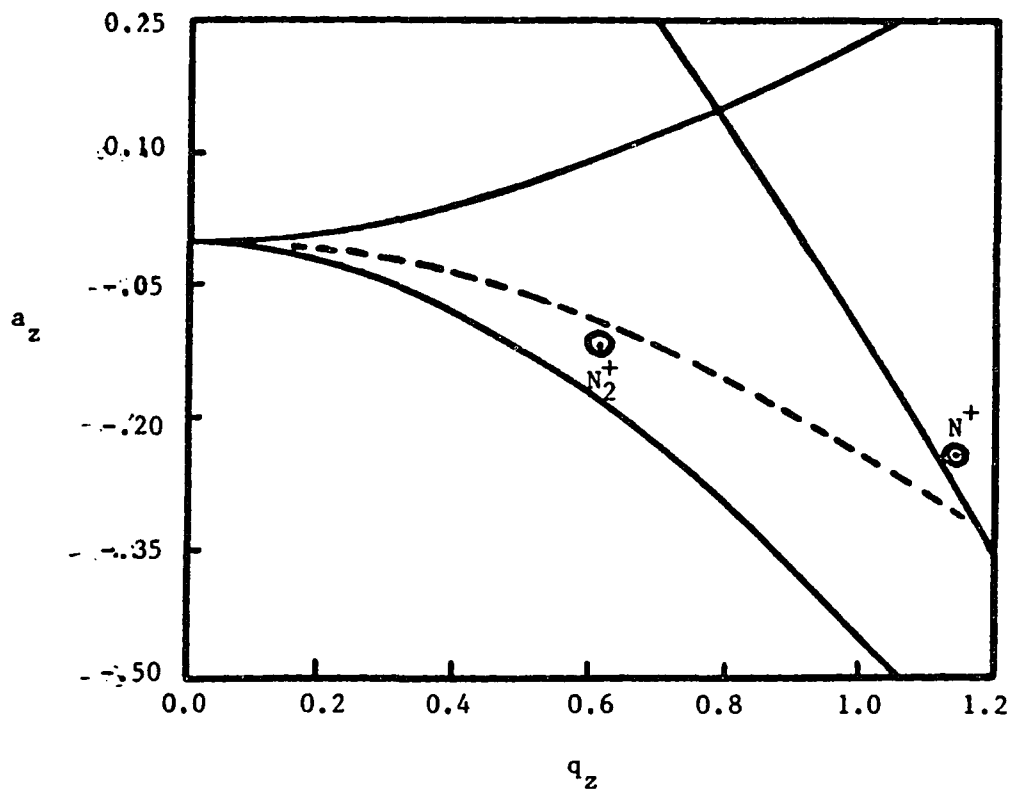
(a)



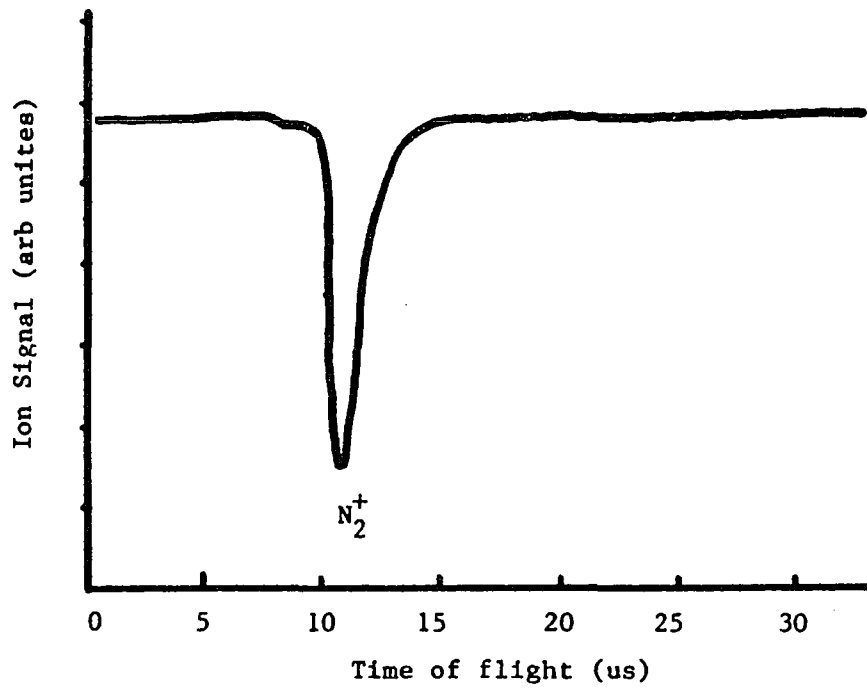
(b)

Fig.(13) (a) Calculated results show that at  $V_0 = 400\text{V}$ ,  $f_0 = 1.2\text{MHz}$ ,  $U_0 = 25\text{V}$   $N^+$  are in the largest density area whereas  $N_2^+$  and  $N^{+2}$  can not be confined.

(b)  $N^+$  signal detected by channel electron multiplier at  $V_0 = 400\text{V}$ ,  $f_0 = 1.2\text{MHz}$ ,  $U_0 = 25\text{V}$



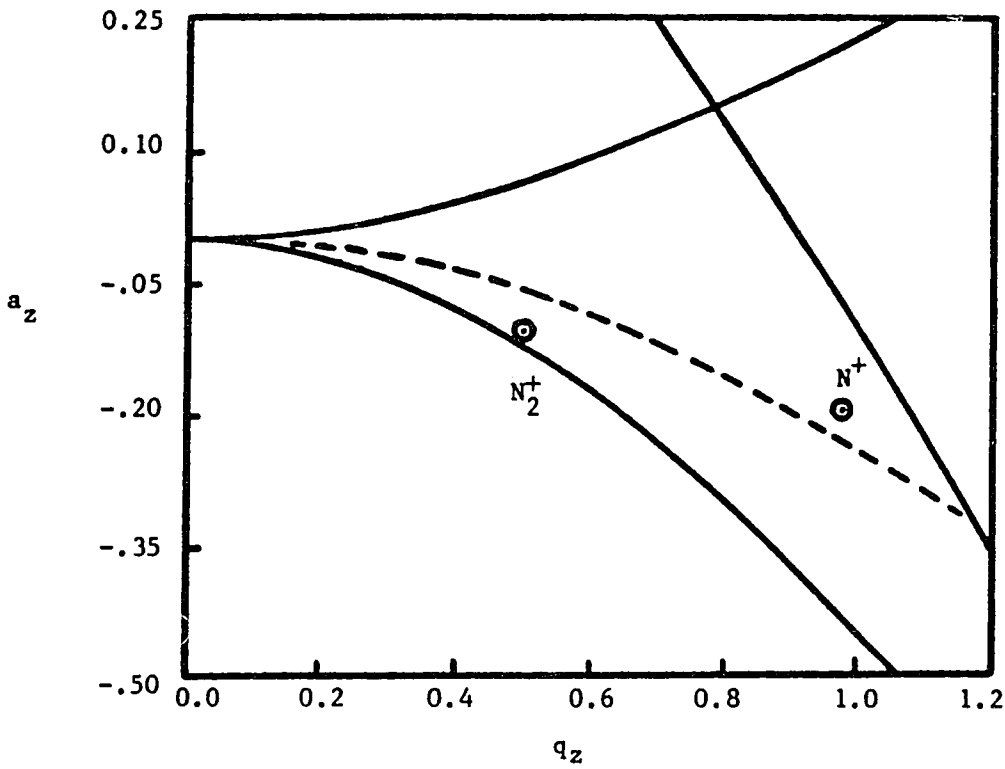
(a)



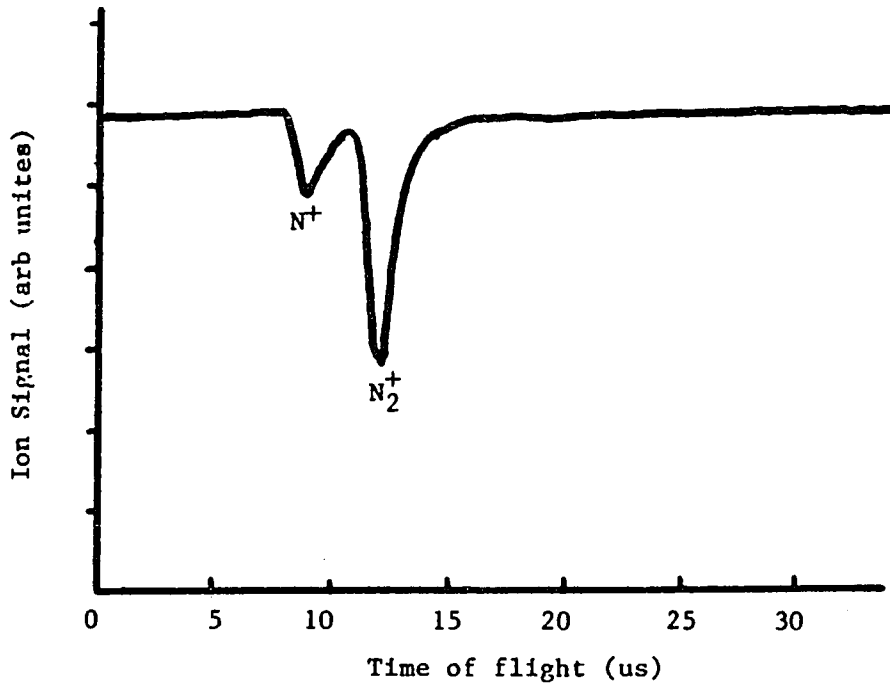
(b)

Fig.(14) (a) Calculated results show that at  $V_0 = 255\text{V}$ ,  
 $f_0 = 0.65\text{MHz}$ ,  $U_0 = 20\text{V}$ , only  $N_2^+$  can be trapped.

(b)  $N_2^+$  signal detected by channel electron multiplier  
at  $V_0 = 255\text{V}$ ,  $f_0 = 0.65\text{MHz}$ ,  $U_0 = 20\text{V}$ .



(a)



(b)

Fig.(15) (a) Calculated results show that at  $V_0 = 220\text{V}$ ,  $f_0 = 0.65\text{MHz}$ ,  $U_0 = 20\text{V}$ , both  $N^+$  and  $N_2^+$  can be confined.

(b)  $N^+$  and  $N_2^+$  signal detected by channel electron multiplier at  $V_0 = 220\text{V}$ ,  $f_0 = 0.65\text{MHz}$ ,  $U_0 = 20\text{V}$ .

equation:

$$t = s \sqrt{\frac{m}{2Vq}} \quad (4.6)$$

where  $s$  is the distance between center of the trap to the CEM,  $V$  is dump pulse voltage, and  $\frac{m}{q}$  is mass to charge ratio of the ions. The experimental results are consistent with the calculations, i.e. when the trap parameters are set to confine both ions, according to the calculated results, we see two ion signals, but when we detune the parameters to store one kind of ion, only one ion signal appeared, and the flight time of those are consistent with Eq.(4.6). When we turn off the  $N_2$  gas supply, no signal was observed.

In this experiment the rf frequency for the ion trap has been set at  $f_0 = 1.2\text{MHz}$ . The rf peak potential  $V_0$  and DC bias  $U_0$  have been scanned to find a optimum storage condition for  $N^+$ , that is, deep spherical well, which will confine  $N^+$  in the relatively larger density with the maximum stability. The largest  $N^+$  signal was observed at  $f_0 = 1.2\text{MHz}$ ,  $V_0 = 400\text{V}$ , and  $U_0 = 25\text{V}$ . These setting were used throughout this experiment.

The storage time of  $N^+$  in the trap with various  $N_2$  pressures was determined by monitoring the decrease of the ion signal magnitude when the stored ions were driven out of the trap at progressively longer delay times. A plot of the decay curves is shown in Fig.(16). The storage time at  $1 \times 10^{-6}\text{Torr}$  was about 1 sec. At higher pressure, storage time decreased. Limitation of the storage time is mainly due to  $N^+$  loss through elastic collisions, the charge transfer process  $N^+(\text{}^5S_2) + N_2 \rightarrow N_2^+ + N$ , and various quenching processes, but in all cases the storage time exceeded the metastable lifetime by at least a factor of 10.

#### 4) Photon Detection

Photons spontaneously emitted from  $N^+(\text{}^5S_2)$  in the ion trap were detected by

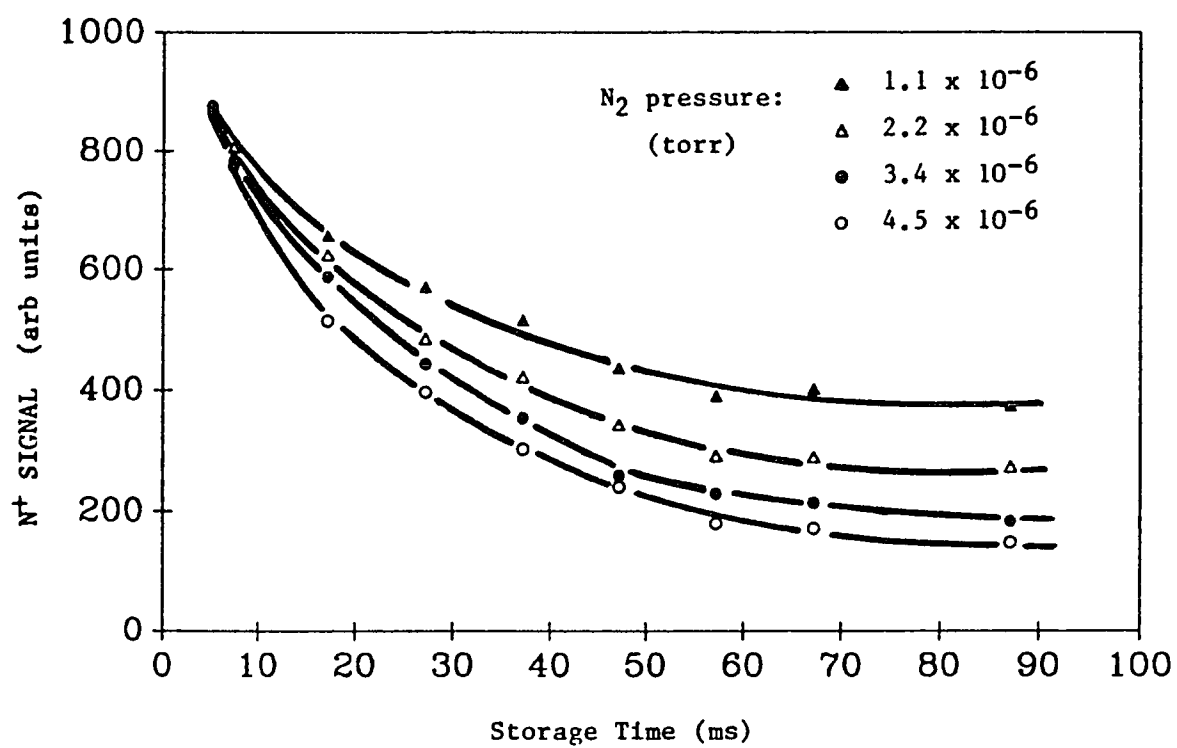


Fig.(16) Normalized decay curves of  $N^+$  signal versus storage time under various  $N_2$  pressures.

a photomultiplier tube (PMT) and the corresponding signal was sent to a gated multichannel analyzer (MCA) where the signal was stored and displayed. The main source of noise in our experiment is the blackbody radiation from the electron gun cathode. An interference filter with  $230\text{\AA}$  bandpass centered at  $2150\text{\AA}$  was used to reduce this noise. An average dark count rate of 0.8 counts per second was typical with the electron gun heater on. Another main noise source is a fast decay ( $\tau < 0.3\text{ms}$ ),<sup>2</sup> which was seen and could attributed to emission in the  $\text{N}_2$  Lyman–Birdge–Hopfield bands. This fast decay was discriminated against by delaying the detection gate with respect to the electron gun pulse. The width of the relaxation pulse was chosen to 1.6ms, which is long enough to avoid the fast decay and compensate e gun bias switching off time. The MCA, which was set at multichannel scaling mode (MCS), was then gated on by the falling edge of the relaxation pulse and started to count the photons seen by the PMT.

In this experiment, 256 channels were selected for the MCS sweep with  $200\mu\text{s}$  per channel. So the total time for one sweep was  $256 \times 200\mu\text{s} = 51.2\text{ms}$ , which is one order of magnitude greater than the estimated  $\text{N}^+(\text{}^5\text{S}_2)$  lifetime. The PMT high voltage was set at 2400V for a  $10^6 \sim 10^7$  amplification factor.

## 5) Data Analysis

Data accumulated by the MCA is dumped to the computer and analyzed by the "DISCRETE" program. Physically, only one exponential decay is allowed for the following reasons:

- a) The trap parameters have been set such that it can only confine  $\text{N}^+$ .
- b) The narrow band filter will only allow photons of about  $\lambda \text{ } 2140\text{\AA}$  to pass through.
- c) Non–intersystem fast decays with photons in the range of  $2000\text{\AA}$  to  $2300\text{\AA}$  are discriminated against by the 1.6ms delay. In other words, the

PMT can only see photons due to  $N^+(^5S_2)$  to  $N^+(^3P_{1,2})$  transition.

The automatic least squares analysis of data can be represented by

$$N_k = \alpha_0 + \alpha_1 \exp(-\lambda_1 t_k) \quad (4.7)$$

where

$$k = 1, 2, \dots, 256$$

$$t_1 = 0.2\text{ms}, \quad \delta t = 0.2\text{ms}$$

and  $N_k$  is the number of photons at time  $t_k$ , whereas  $\lambda_1$  is the  $^5S_2$  decay rate.

## V EXPERIMENTAL RESULTS

Six sets of measurements, taken at different  $N_2$  pressures ranging from  $1 \times 10^{-6}$ Torr to  $5 \times 10^{-6}$ Torr, were used to obtain the final results. All other parameters were fixed. Every measurement of the radiative transition rate under certain  $N_2$  pressure was the mean value of several runs. The standard deviation was calculated afterwards. The count rate as a function of time varies with the  $N_2$  pressure. At  $5 \times 10^{-6}$ Torr the count rate was 29.6 counts per second at channel 15 (recall the sweep time was 200  $\mu$ s per channel ) which is about one lifetime. A decay curve with good signal to noise ratio could be obtained in 6 to 14 runs with 9999 sweep cycles per run. Here one sweep cycle represents one measurement, so the data were accumulated up to 140000 measurements. A typical  $N^+(^5S_2)$  decay curve is shown in Fig.(17), where a nonlinear, least-squares routine with a function of the form  $\alpha_0 + \alpha_1 \exp(-\lambda_1 t_k)$  was used to fit the data. The results of the fit are shown in the following table

$N_2$ Pressure (torr)	Decay Rate ( $\text{sec}^{-1}$ )
$1.0 \times 10^{-6}$	$190 \pm 10$
$1.5 \times 10^{-6}$	$214 \pm 11$
$2.0 \times 10^{-6}$	$230 \pm 11$
$3.0 \times 10^{-6}$	$270 \pm 13$
$4.0 \times 10^{-6}$	$297 \pm 13$
$5.0 \times 10^{-6}$	$342 \pm 19$

where three standard deviation has been chosen to ensure the results with confidence of 99%.



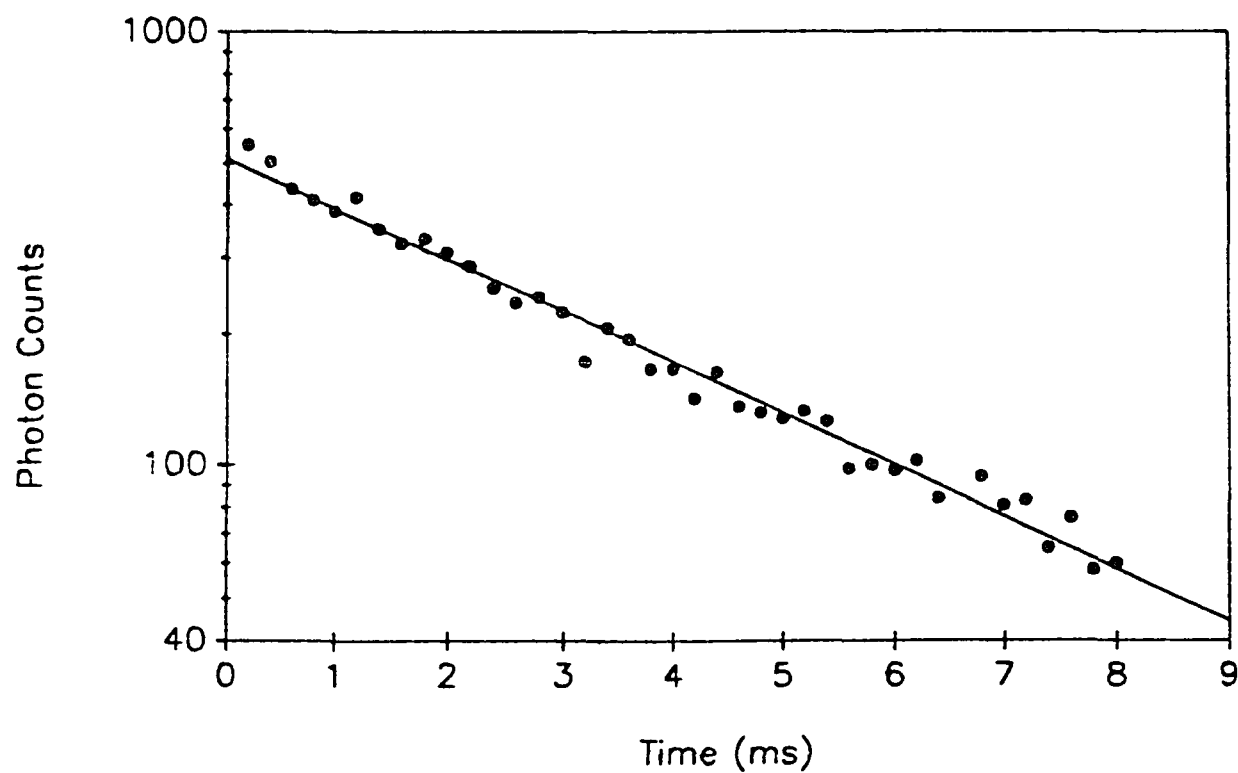


Fig.(17) A typical  $N^+(^5S_2)$  decay curve. The straight line is the least-squares fit to this decay.

Different radiative transition rates with respect to the different  $N_2$  pressures implies loss of metastable ions due to various channels of quenching, elastic collision and charge transfer. Fig.(18) shows the relation between decay rate and  $N_2$  pressure. The slope of the decay rate versus the  $N_2$  pressure curve gives a total ion loss rate coefficient of  $1.14 \times 10^{-9} \text{cm}^3 \text{sec}^{-1}$  for  $N^+(^5S_2)$  in  $N_2$ . This curve was found to be linear in our  $N_2$  pressure range, as expected. By extrapolating the curve to zero  $N_2$  pressure, we get the mean  $N^+(^5S_2)$  decay rate of  $156 \pm 17 \text{sec}^{-1}$ .

The whole system for this experiment was carefully tested and calibrated. The MCA timing in multichannel scale mode was calibrated by 7104 oscilloscope calibrator for which the deviation at repetition rate of 1kHz was within 0.25%. The ion trap rf frequency was monitored by Ortec 878 timer/counter during the experiment. It was quite stable and the deviation was less than 0.01%. The ion trap power supplies both AC and DC were also monitored by 2235 oscilloscope to insure the ion trap operating point was right. The working condition of the e gun is also very critical to this experiment. That includes: electron gun filament heater current, electron gun positive and negative bias voltage, and electron gun electron firing stability. If the electron gun filament potential is too high, excessive electrons could go into the ion trap during electron gun "on" time. These excess electrons could partly short the end cap to the ring electrode of the ion trap thus changing the RF amplitude  $V_o$  and disturbing  $N^+$  ion storage. On the other hand, if the filament heater current is too low, the number of electrons created by electron gun will not be enough to generate sufficient  $N^+$  so that the signal to noise ratio will be poor. To avoid that, we monitored the trap RF amplitude  $V_o$  as we increased the electron gun heater current so that the current could reach a threshold without changing the  $V_o$ . The electron gun negative bias was set in between the electron gun and the end cap of ion trap to drive the electrons created by electron gun into the ion trap during the electron gun "on" time, as mentioned in III. The magnitude of the negative bias

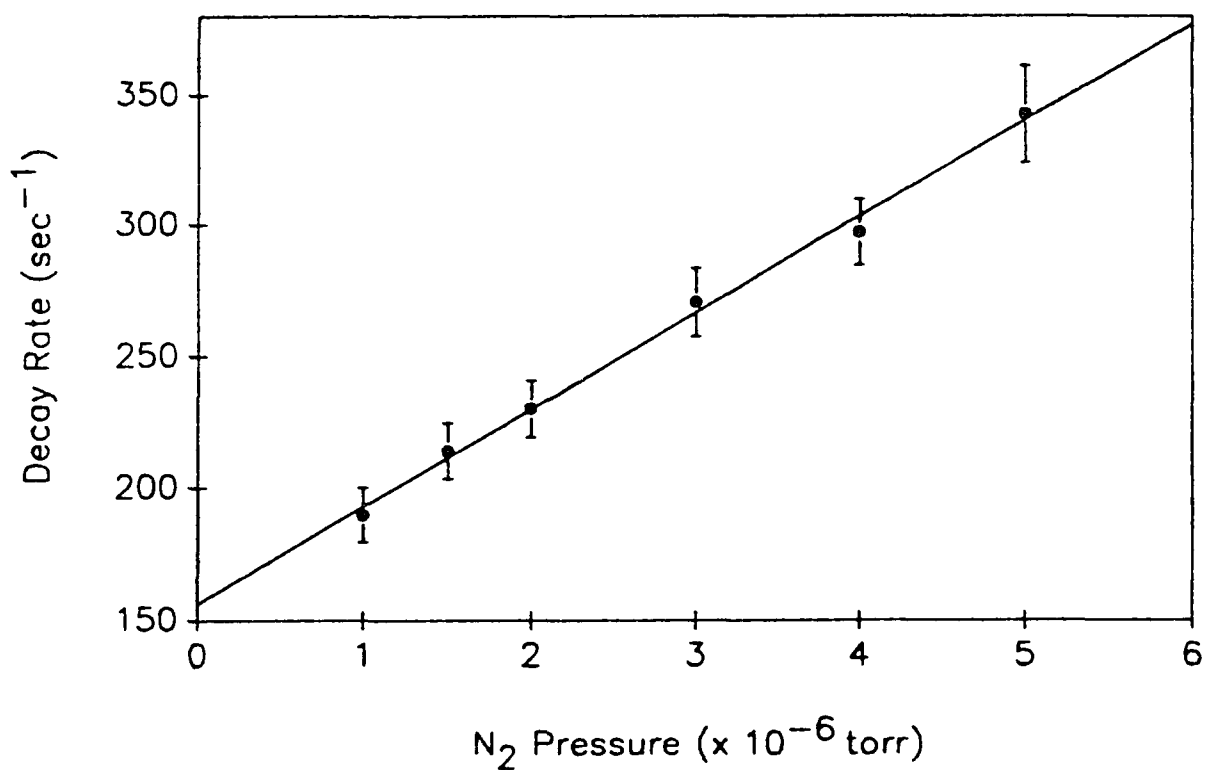


Fig.(18)  $N^+$  decay rate vs  $N_2$  pressure. The slope of the decay rate vs  $N_2$  gives a nonradiative quenching plus ion loss rate coefficient of  $1.14 \times 10^{-9} \text{cm}^3 \text{sec}^{-1}$  and zero extrapolation gives  $N^+(^5S_2)$  decay rate  $A_{\text{rad}} = 156 \pm 17 \text{sec}^{-1}$ .

voltage was chosen to get the maximum  $N^+(^5S_2)$  radiation. The electron gun positive bias was set to hold the electrons during the electron gun "off" time. This voltage should be high enough so that no electrons can escape from the electron gun and get into the ion trap to produce more ions during electron gun "off" time, otherwise the new born  $N^+(^5S_2)$  may compensate the original  $N^+(^5S_2)$  decay, that could make the "lifetime" looks longer. To optimize this, several different positive bias voltages were set and the decay rates were measured. No difference was found in the decay rate whether +50v or +100v bias was used. To make the electron gun firing stable, we usually activate the electron gun a few hours before we do the measurement. Since we got the lifetime by extrapolating the decay rate to zero—pressure, the linearity of the pressure measurement is also very important. This has been done by comparing the Masstorr DX100 to an ion gauge. Though the ion gauge was not carefully calibrated this did not affect the decay rate, which depends only upon the linearity of the ion gauge. Compared with the systematic error, the statistical error was dominant in this work. So consequently, the measured value for the radiative decay rate of  $N^+(^5S_2)$  is  $A_{\text{rad}} = 156 \pm 17 \text{ sec}^{-1}$ , or, equivalently, the radiative lifetime is  $\tau_{\text{rad}} = 6.4 \pm 0.7 \text{ msec}$ .

This result is in very good agreement with the theoretical values, but about 34% longer than the first measurement made by Knight. A reasonable explanation for this difference is that the ion trap we used is slightly different than that of Knight's. In our experiment, a meshed ion trap was used. Unwanted ions created in the ion trap during e gun "on" time, will more easily to get out of this ion trap than the ion trap with a solid wall during the "relax" time so that there would be less disturbance to the lifetime measurement. The pressure in the ion trap, after the creation of ions, tended to quickly equalize with the surroundings so that the pressure we read from the Masstorr DX100 was the same as the pressure in the ion trap during the lifetime measurement. Our residual gas pressure was very low

( $5 \times 10^{-9}$ Torr) so the quenching from the residual gas can be neglected. We noticed that Knight used a solid wall ion trap in his measurement. This kind of trap does not have the advantages of the meshed ion trap. The residual gas pressure was  $1.8 \times 10^{-7}$ Torr in Knight's system so there were possibilities that some unknown quenching may happen during the lifetime measurement. Especially, if there is any contamination on the ion trap wall and they keep to vaporize in a certain rate during the lifetime measurement, these unwanted particles could then interact with the desired ions and cause additional ion loss. Such unpredictable ion loss may make the "lifetime" shorter. The pressure in the ion trap during the measurement could also be higher than the surroundings and the pressure read from the ion gauge could be different from that in the ion trap. The shift of the pressure could also affect the decay rate measurement.

## VI. CONCLUSION

- 1) We created  $N^+(^5S_2)$  via electron impact with  $N_2$  gas in a cylindrical rf-quadrepole ion trap.
- 2)  $N^+$  has been confined in the ion trap for at least ten times longer than the  $N^+(^5S_2)$  radiative lifetime under  $1 \times 10^{-6}$ Torr to  $5 \times 10^{-6}$ Torr  $N_2$  pressure.
- 3)  $N^+(^5S_2)$  to  $N^+(^3P_{1,2})$  radiative decay has been detected. The lifetime of the  $N^+(^5S_2)$  metastable state is  $6.4 \pm 0.7$  msec.

Our experimental results confirmed the theory of the  $N^+(^5S_2)$  decay. It also supported the interpretation of the  $\lambda$  2145 $\text{\AA}$  auroral feature as being due to  $N^+(^5S_2)$  emission.

## REFERENCES

1. Physics Through The 1990s, National Academy Press, Washington D.C. 1986
2. K. A. Dick, Geophys. Res. Lett. 5, 273 (1978).
3. R. D. Knight, Phys. Rev. Lett. 48, 792, 1982.
4. A. Dalgarno, G. A. Victor, and T. W. Hartquist,  
Geophys. Res. Lett. 8, 603, 1981.
5. A. Hibbert and D. R. Bates, Planet. Space Sci. 29, 263, 1981.
6. P. W. Erdman, P. J. Espy, and E. C. Zipf, Geophys. Res. Lett. 8, 1163, 1981.
7. W. E. Sharp, Geophys. Res. Lett. 5, 703, 1978.
8. D. Feldman, Geophys. Res. Lett. 3, 9, 1976.
9. Personal Communication
10. A. G. Calamai and C. E. Johnson, Bulletin of the American Physical Society,  
950, 1988.
11. C. C. J. Roothaan, and P. S. Kelly, Phys. Rev. 131, 1177, 1963.
12. W. Paul, and H. Steinwedel, German Patent No. 944, 900, June 28, 1956
13. K. Berkling, "Diplomarbeit", Physik. Inst. Univ. Bonn, German, 1956
14. E. Fischer, Z. Physik. 156, 26, 1959
15. P. H. Dawson, and N. R. Whetton, Dyn. Mass Spec., 2, 1, 1971.  
P. H. Dawson, Int. J. Mass Spec. Ion Phys., 14, 317, 1974.  
P. H. Dawson, and M. Meunier, Int. J. Mass Spec. Ion Phys., 29, 269, 1979.  
P. H. Dawson, and C. Lambert, J. Vac. Sci. Tech., 12, 941, 1975.
16. P. H. Dawson, and N. R. Whetton, J. Vac. Sci. Tech., 5, 1, 1968.
17. P. H. Dawson (ed.), "Quadruple Mass Spectrometer and Its Applications",  
Elsevier Scientific Pub. Co., New York, 1976
18. P. H. Dawson, and C. Lambert, Int. J. Mass Spec. Ion Phys., 16, 269, 1975.
19. P. H. Dawson, and C. Lambert, Int. J. Mass Spec. Ion Phys., 14, 339, 1974.

- J. F. J. Todd, and R. M. Waldren, *Int. J. Mass Spec. Ion Phys.*, 29, 301, 1979.
- J. E. Fulford, and R. E. March, *Int. J. Mass Spec. Ion Phys.*, 30, 39, 1979.
20. P. H. Dawson, and N. R. Whetton, *J. Vac. Sci. Tech.*, 5, 11, 1968.
21. P. H. Dawson, J. W. Hedman, and N. R. Whetton,  
*J. Sci. Ins.*, 40, 1444, 1969.
22. P. H. Dawson, and N. R. Whetton, *Adv. Electron Phys.*, 27, 59, 1969.
23. G. Lawson, and J. F. J. Todd, *Chem. in Brit.*, 8, 373, 1972.
- J. F. J. Todd, R. M. Waldren, R. E. Mather, and G. Lawson,  
*Int. J. Mass Spec. Ion Phys.*, 28, 141, 1978.
- R. E. Mather, G. Lawson, and J. F. J. Todd,  
*Int. J. Mass Spec. Ion Phys.*, 28, 347, 1978.
24. R. M. Waldren, and J. F. J. Todd, *Int. J. Mass Spec. Ion Phys.*, 29, 315, 1979.
25. G. Lawson, R. F. Bonner, and J. F. J. Todd, *J. Phys. E: Sci. Ins.*, 6, 357, 1973.
26. M. Benalin, and Clande, *Int. J. Mass Spec. Ion Phys.*, 11, 421, 1973.
27. H. G. Dehmelt, *Adv. At. Mol. Phys.*, 3, 53, 1967.
28. R. D. Knight, Ph.D. thesis, University of California, Berkeley, 1979.
29. R. D. Knight, *Int. J. Mass Spec. Ion Phys.*, 51, 127, 1983.
30. R. F. Wuerker, H. Shelton, and R. V. Langmuir, *J. Appl. Phys.*, 30, 342, 1959.
31. R. Iffländer, and G. Werth, *Fifth Inter. Conf. Atom. Phys.*, 1976.
32. M. Baril, and A. Septier, *Rev. de Phys. Appl.*, 9, 525, 1974.
33. S. W. Provencher, "DISCRETE—A program for the automatic analysis of  
multicomponent exponential decay data"  
Max—Planck—Institute für biophysikalische Chemie  
D—3400 Gottingen—Nikolausberg, Federal Republic of Germany, 1976.
34. L. Delenau, and J. A. D. Stockdale, *J. Chem. Phys.*, 63, 3898, 1975
35. John C. Slater, *Quantum Theory of Atomic Structure*, vol. I, II.  
McGraw—Hill Book Company, Inc. 1960



36. VG Gas Analysis LTD, Masstorr DX100 Manual, 1986